

The role of regional circulation features in regulating El Niño climate impacts over southern Africa: a comparison of the 2015/16 drought with previous events

Article (Accepted Version)

Blamey, R C, Kolusu, S R, Mahalela, P, Todd, M C and Reason, C J C (2018) The role of regional circulation features in regulating El Niño climate impacts over southern Africa: a comparison of the 2015/16 drought with previous events. *International Journal of Climatology*, 38 (11). pp. 4276-4295. ISSN 1097-0088

This version is available from Sussex Research Online: <http://sro.sussex.ac.uk/id/eprint/75135/>

This document is made available in accordance with publisher policies and may differ from the published version or from the version of record. If you wish to cite this item you are advised to consult the publisher's version. Please see the URL above for details on accessing the published version.

Copyright and reuse:

Sussex Research Online is a digital repository of the research output of the University.

Copyright and all moral rights to the version of the paper presented here belong to the individual author(s) and/or other copyright owners. To the extent reasonable and practicable, the material made available in SRO has been checked for eligibility before being made available.

Copies of full text items generally can be reproduced, displayed or performed and given to third parties in any format or medium for personal research or study, educational, or not-for-profit purposes without prior permission or charge, provided that the authors, title and full bibliographic details are credited, a hyperlink and/or URL is given for the original metadata page and the content is not changed in any way.

The role of regional circulation features in regulating El Niño climate impacts over southern Africa: A comparison of the 2015/16 drought with previous events

Journal:	<i>International Journal of Climatology</i>
Manuscript ID	JOC-17-0566.R3
Wiley - Manuscript type:	Research Article
Date Submitted by the Author:	06-Apr-2018
Complete List of Authors:	Blamey, Ross; University of Cape Town, Department of Oceanography Kolusu, Seshu; University of Sussex, Geography Mahlalela, Precious; University of Cape Town, Oceanography Todd, M; University of Sussex, Geography Reason, Chris; UCT, Oceanography;
Keywords:	Teleconnections (AO, NAO, MJO, ENSO, SSW, ONI, ADO, MJO) < 4. Geophysical sphere, Drought, Dynamic/Processes < 1. Tools and methods
Country Keywords:	South Africa, Zimbabwe, Angola, Botswana, Mozambique

SCHOLARONE™
Manuscripts

1 **The role of regional circulation features in**
2 **regulating El Niño climate impacts over**
3 **southern Africa: A comparison of the 2015/16**
4 **drought with previous events**

5
6 R. C. Blamey^{1*}, S. R. Kolusu², P. Mahlalela¹, M.C. Todd² and C. J. C. Reason¹

7
8 ¹ *Department of Oceanography, University of Cape Town,*
9 *Private Bag X3, Rondebosch, 7701, South Africa*

10
11 ² *Department of Geography, University of Sussex,*
12 *Brighton, East Sussex BN19RH, UK*

13
14
15
16
17
18
19
20
21
22
23 **Keywords:** Droughts, southern Africa, El Niño, Angola Low, Botswana High, tropical-
24 extratropical connections

25
26

* *Corresponding author address:* Ross Blamey, Dept. of Oceanography,
University of Cape Town, Private Bag X3, Rondebosch, 7701, South Africa
E-mail: ross.blamey@uct.ac.za

ABSTRACT

Extremely dry conditions were experienced across most of southern Africa during the austral summer (October-March) of 2015/16, associated with one of the strongest observed El Niño events in the Pacific. Dry conditions peaked in the early austral summer months (October-December) producing the most intense drought in the 116 year historical record, as measured by the intensity of the Standardized Precipitation Index across all spatial scales up to the sub-continental. We estimate the return period of this extreme early summer drought to be greater than 200 years. The interior and eastern parts of South Africa were particularly hard-hit with station data showing rainfall totals being at their lowest since at least 1950. The early summer dry conditions make the 2015/16 event atypical compared to past El Niño events of similar magnitude. We find that key regional circulation patterns, influenced by planetary scale processes, play an important role in modulating the spatial and temporal evolution of the summer rainfall during these El Niño events. Specifically, (i) the Angola Low and the South Indian Ocean High, two dominant low level circulation features that drive moisture convergence to support convective precipitation in the region, were anomalously weakened in early austral summer of 2015/16 resulting in less moisture being transported over the continent, and (ii) the mid-level Botswana High was stronger than in previous El Niño years further producing unfavourable conditions for rainfall through stronger subsidence in the mid- to upper levels over southern Africa.

1. Introduction

During the austral summer wet season of 2015/16 (October-March), exceptionally dry conditions occurred across southern Africa. SADC (2016a,b) reported widespread and severe impacts across many sectors including considerable loss of crops and livestock, which drove an increase in food prices, severe water shortages and resulting water restrictions (notably in South Africa), and reduced electricity generation and supply. SADC declared a regional drought disaster and, by September 2016, six SADC countries had declared national drought emergencies (Botswana, Namibia Lesotho, Malawi, Swaziland and Zimbabwe) and in South Africa the drought emergency status was declared for seven of the county's nine provinces, with a temporary red alert also declared for central and southern provinces of Mozambique. Droughts are not uncommon in southern Africa, (Mulenga *et al.*, 2003; Rouault and Richard 2003; Reason *et al.*, 2005) and the local socio-economic impacts can be severe due to a semi-arid climate with high space-time variability (Richard and Pocard 1998; Rouault and Richard 2003), and the dependence of much of the rural population on rain-fed subsistence agriculture. Thus, drought is viewed as the principal type of natural disaster across Africa and a common trigger for household insecurity (Calow *et al.*, 2010).

Subtropical southern Africa, defined here as Africa south of 15°S, has a complex climate system with strong zonal and meridional climate gradients related to topography and adjacent oceans, and pronounced variability related to both local and remote forcing. El Niño-Southern Oscillation (ENSO) is the dominant mode of interannual climate variability globally and it is widely accepted as the mode with the greatest impact on southern Africa during the summer, the main rainy season (Lindesay, 1988; Rocha and Simmonds, 1997; Reason *et al.*, 2000; Cook, 2001; Reason and Jagadheesha, 2005). Droughts in southern Africa are often associated with El Niño events (Lindesay, 1988; Rocha and Simmonds, 1997; Reason *et al.*,

2000; Cook, 2000; Reason and Jagadheesha, 2005; Lyon and Mason, 2007), but the underlying mechanisms through which the dry conditions are created are not completely understood. Furthermore, not all El Niño events lead to widespread drought in southern Africa and not all droughts occur during El Niño years.

76

During El Niño, unfavourable rainfall conditions occur over southern Africa through circulation changes that lead to less moisture convergence, uplift and instability which influence tropical-extratropical cloudband development (Cook, 2001; Mulenga *et al.*, 2003; Ratnam *et al.*, 2014). These cloudbands, locally known as tropical-temperate troughs (TTT), often extend NW-SE over southern Africa from the Angolan Low region out into the southwest Indian Ocean (Harrison, 1984; Todd and Washington, 1999; Washington and Todd, 1999; Fauchereau *et al.*, 2009; Hart *et al.*, 2010; Manhique *et al.*, 2011; Hart *et al.*, 2013). Cloudbands are large contributors to South African summer rainfall and are associated with local heavy rainfall events (Harrison, 1984; Hart *et al.*, 2010; Hart *et al.*, 2013). The preferred axis of these TTT cloudbands constitutes the South Indian Ocean Convergence Zone (SIOCZ) (Cook, 2000; Lazenby *et al.*, 2016).

88

The regional circulation (Fig. 1) supplies moisture convergence from the surrounding oceans into the mean SIOCZ. It is the zonal wind convergence between the westerlies from the tropical Atlantic around the Angolan Low, easterlies from the southwest Indian Ocean around the subtropical South Indian Ocean High Pressure (SIHP) and northeasterlies from the equatorial western Indian Ocean that forms the boundary of the SIOCZ (Cook, 2000) and supplies specific TTT events (Todd and Washington, 1999). As such, a stronger (weaker) Angolan Low and SIHP has been linked to an increase (decrease) in rainfall across the region (Cook *et al.*, 2004; Reason and Jagadheesha, 2005; Reason *et al.*, 2006; Manhique *et al.*,

2011; Munday and Washington, 2017). During El Niño events, it is thought that this SIOCZ shifts northeastwards due to weakening of the SIHP resulting from ENSO-generated atmospheric Rossby waves in the Southern Hemisphere, resulting in dry conditions prevailing over southern Africa (Cook, 2001; Fauchereau *et al.*, 2009; Ratnam *et al.*, 2014).

The reduction of moisture and associated circulation anomalies over the continent during El Niño is only one of the mechanisms by which unfavourable conditions for rainfall occur. Another regional feature of importance is the mid-level Botswana High which forms, on average, in spring to the southwest of the high rainfall area of the Congo Basin and shifts south and strengthens during the summer (Reason, 2016; Driver and Reason, 2017). This mid-level high, thermally induced in response to heat released by tropical regions of high rainfall, has a strong relationship to rainfall patterns across southern Africa. The Botswana High also tends to be stronger (weaker) during El Niño (La Niña) events, with the magnitude in the anomaly not necessarily being in proportional to the strength of the ENSO event.

The influence ENSO has on southern African circulation is thought to occur through modulation of the local Africa-Indian Ocean sector Walker Circulation, from large-scale wave responses to Pacific heating and to SST anomalies in the Indian and Atlantic Oceans. Under typical El Niño conditions, the anomalous Pacific equatorial heating drives anomalous heat-induced circulations in the tropics, known as the Matsuno-Gill response (Matsuno, 1966; Gill, 1980). This results in equatorially symmetric anticyclonic circulation anomalies in the Indian Ocean in the lower levels of the atmosphere and anomalous anticyclonic circulation present over southern Africa during December - February (Reason *et al.*, 2000; Ratnam *et al.*, 2014). SST anomalies in the Indian and Atlantic Oceans can modulate southern African climate through their influence on these circulation features. El Niño events typically involve

warming across the tropical Indian and Atlantic Oceans. Goddard and Graham (1999) highlight the importance of Indian Ocean SSTs in driving the north-south dipole in rainfall anomalies over East Africa/southern Africa associated with ENSO warm and cold events. Other regional SST modes of importance include the subtropical Indian Ocean dipole (Behera and Yamagata, 2001; Reason, 2001) and, to a lesser extent, the Indian Ocean dipole (Saji *et al.*, 1999; Yamagata *et al.*, 2003; Behera *et al.*, 2005). The background state of SSTs in these important regions will vary between different El Niño events and will likely modulate the effect of signals emanating from the Pacific (e.g. Hoell *et al.*, 2017). Preethi *et al.*, (2015) have documented that the rainfall response over Africa differs depending on the type of ENSO event (i.e. Central Pacific versus Eastern Pacific El Niño) and the background state of SSTs in the Indian Ocean.

ENSO can also influence southern African circulation through extra-tropical atmosphere teleconnections. The Pacific South American (PSA) pattern (Karoly, 1989; Ghil and Mo, 1991; Mo and Higgin, 1998; Mo, 2000) which is characterized by an alternating Rossby wave-train of pressure/height anomalies originating from the tropics during ENSO events, leads to substantial atmospheric circulation and SST anomalies in the southeast Atlantic / southern Africa region (Colberg *et al.*, 2004). The peak in amplitude of the PSA anomalies during ENSO phases typically takes place during the austral spring (September-November), compared to the ENSO related tropical SST anomalies peaking later during the austral summer (December-February; DJF) (Jin and Kirtman, 2009; Schneider *et al.*, 2012). The interaction between the anomalous wave flux from the South Pacific and the Southern Hemisphere westerly jet leads to an anomalous anticyclonic circulation over southern Africa during El Niño events (Ratnam *et al.*, 2014).

The relationship between Pacific SSTs and extra-tropical regions is also evident through the influence ENSO has on the Southern Annular Mode (SAM) (Seager *et al.*, 2003; Carvalho *et al.*, 2005; L'Heureuz and Thompson, 2006; Fogt and Bromwich, 2006; Schneider *et al.*, 2012) and/or the modulation of ENSO by SAM (e.g. Fogt *et al.*, 2011; Cai *et al.*, 2013; Prabhu *et al.*, 2016; Prabhu *et al.* 2017). The mid-latitude westerlies typically extend further equatorwards during negative SAM and the reverse during positive SAM. This shift in storm tracks, coupled with anomalous wind patterns, leads to contrasting rainfall patterns across South Africa, with the winter rainfall region associated with anomalously dry (wet) conditions and the summer rainfall region being anomalously wet (dry) during the positive (negative) phase of the SAM (Reason and Rouault, 2005; Gillett *et al.*, 2006). The links between the SAM and PSA during ENSO events have only been investigated recently. Anomalous heating in the tropics may strengthen the meridional temperature gradient thereby enhancing the subtropical jets, which act as waveguides to steer transient eddies on a more equatorward and zonal path than that of the mean climatological flow (Seager *et al.*, 2003; L'Heureuz and Thompson, 2006).

Despite much research into ENSO impacts on southern Africa, a complete understanding remains elusive. As summarised above, a number of important regional scale features have been identified as exerting important controls on rainfall, which themselves may be influenced by forcing from the tropical Pacific. In this paper, we explore the role of regional circulation features in modulating the nature of impacts over southern Africa from remote Pacific El Niño events. To this end we compare, over the course of the early and late wet season, the rainfall and the drought intensity over southern Africa during the three strongest El Niño events since 1979. This comparison is of interest since one of these three strongest events (1997/1998) did not lead to the expected severe drought over the region while there

were important differences in the timing and extent of the droughts in 1982/83 and 2015/16. This comparison is followed by an investigation of the key candidate mechanisms of teleconnection and regional circulation systems (Fig. 1) responsible for the rainfall conditions experienced during each event. Exploring how regional controls influence weather and climate patterns across southern Africa may provide insight into the predictability of the local impacts during strong El Niño events and potentially improve seasonal forecasting.

2. Datasets and Methodology

Monthly SST data were obtained from the NOAA Optimum Interpolated Sea Surface Temperature V2 (OISST) on a $1.0^{\circ} \times 1.0^{\circ}$ horizontal grid (Reynolds *et al.*, 2002). Historical El Niño events are typically identified when the 5-month running average of SST anomalies averaged over the Niño-3.4 region (5°S – 5°N ; 120° – 170°W) exceeds 0.5°C for at least six consecutive months (Lyon and Mason, 2007). Figure 2 depicts the seasonal evolution of the monthly SST anomalies for the El Niño events so identified, and highlights the three strongest El Niño events, 1997/98, 2015/16 and 1982/83 which are the focus of this study.

The analysis focuses on the austral summer of October–March (ONDJFM) and distinguishes between early (October–December; OND) and late summer (January–March; JFM). To evaluate drought intensity the Standardized Precipitation Index (SPI) (McKee *et al.*, 1993) was used. The SPI is a multi-scalar, probabilistic drought indicator, designed to quantify the precipitation surplus/deficit over multiple timescales. It is obtained by fitting a Gamma distribution (Thom, 1958) to monthly GPCC precipitation values. A drought event is considered to occur when the SPI falls below -1 and extreme and exceptional drought conditions are indicated by SPI values less than -1.5 and -2, respectively (McKee *et al.*, 1993).

197

198 The areal extent and intensity of 3-month SPI were determined using Intensity-Areal-extent
199 Frequency (IAF) curves (Mishra and Singh, 2009; Mishra and Cherkauer, 2010). IAF curves
200 express the relationship between intensity and spatial extent of SPI-indicated drought, and
201 allow comparison between years, irrespective of the precise spatial location of drought within
202 the study domain. IAF curves were derived for the OND (SPI-3) and ONDJFM (SPI-6)
203 season by calculating the mean SPI over the full range of spatial extents within southern
204 Africa (10° - 35° S, 10° - 40° E); defined by percentiles of the spatial distribution of all grid cells
205 in the domain (i.e. the mean SPI over the lowest 5%, 10%, 20% ... 100% of ranked SPI grid
206 cell values within the domain).

207

208 We compare the observed SPI IAF curve for the extreme 2015/16 El Niño event with IAF
209 curves representing 'benchmark' return periods. Estimating return periods of drought events
210 is challenging given the relatively short observational record for what are relatively long
211 duration events. To increase our sample of climate events beyond the observed record we use
212 large ensembles of climate model simulations from the HAPPI experiment (Mitchell et al.,
213 2017), designed specifically to quantify climate extremes, through the use of relatively high
214 model resolution and large initial-condition ensembles. We use precipitation data from four
215 atmospheric models, namely HadGEM3, CAM5, MIROC5 and NORESM, (degraded to
216 common resolution of 1°) each with 10 ensemble members, run over the period ~1950s-
217 2010s, forced with observed SSTs and 'historical' greenhouse gases and aerosol radiative
218 forcings. These simulations provide about 2400 years of simulated data. As with the
219 observations we derive the mean SPI-3 (and SPI-6) for each areal extent interval (5^{th} , 10^{th} ,
220 etc. spatial percentiles over the domain), for each of the ~2400 model years. Estimation of
221 return periods is based on the Extreme Value Theory (EVT), widely used for the description

of rare climate events in the extreme tail of the parameter distribution. The Generalized Extreme Value distribution (GEV) is fitted to the distribution of extreme SPI values, for each areal extent separately (using maximum likelihood estimation and a chi-squared goodness-of-fit test, Coles *et al.*, 2001). This distribution of extremes ('block maxima') is composed of the most intense drought values (the maximum SPI*-1) within non-overlapping 'blocks' of 30 years, a standard climatological period. Then, return periods are estimated by inverting the resulting GEV cumulative probability distribution for a range of periods from 30-300 years, for each areal extent separately, providing IAF curves for benchmark return periods (see Fig. 4). Finally, the return period of the 2015/16 El Niño event itself was estimated from the closest match (based on least squared error) of the observed 2015/16 IAF curve with the various benchmark IAF return period curves. Whilst our approach is similar to previous drought analyses (e.g. Robeson, 2015) we recognise a number of caveats. First, the estimated return periods are sensitive to the arbitrary choice of block size and we estimate the uncertainty associated with this using periods of 25-60 years. Second, whilst the large ensembles provided by the HAPPI experiment are designed specifically for analysis of extremes they necessarily provide only a partial representation of the climate variability 'space'.

At the local scale, daily precipitation data from the South African Weather Service (SAWS) for January 1950 to March 2016 were analysed using only those stations with 95% of the record available. Six boxes were subjectively determined from these data to represent different parts of the South African summer rainfall region (see Fig. 1); namely, Limpopo (A), Gauteng (B), Free State (C), north coastal KwaZulu-Natal (KZN) (D); south coastal KZN (E) and the Eastern Cape (F). These data were averaged to monthly data and then standardized anomalies derived for each region. Due to the unavailability of station data for other countries, the 1° resolution Global Precipitation Climatology Centre (GPCC) dataset

was used for southern Africa as a whole (Schneider *et al.*, 2014). In order to cover the full period, the GPCC *Full Data Product* v7 (1901-2010; Schneider *et al.*, 2011a) was combined with the GPCC *V4 monitoring product* (Schneider *et al.*, 2011b), which is available from 2007 to present.

For analysis of regional circulation patterns we use data from the National Center for Environmental Prediction (NCEP) - Department of Energy (DOE) Second Atmospheric Model Intercomparison Project (AMIP-II) reanalysis data (Kanamitsu *et al.*, 2002), at a resolution of 2.5° and six hours from 1979 onwards. This reanalysis is thought to perform better than other products over southern Africa (Zhang *et al.*, 2013; Moalafhi *et al.*, 2016). Moisture fluxes were computed from the horizontal winds and specific humidity. The statistical significance of the composite average geopotential height anomalies was determined at each grid point using a Student's *t* method for testing against the null hypothesis that the actual composite anomaly is zero.

To define the Angola Low, a criterion of the lowest 10% of 850 hPa geopotential height for OND and JFM was used. An average of the 850 hPa geopotential height within a box surrounding the Angola Low (see Fig. 1 for location) is then used to create an Angola Low index. The latitudinal extent of the box domain is restricted in order to exclude the influence of the Kalahari Heat Low to the south and equatorial convergence to the north (Munday and Washington, 2017).

3. Regional rainfall anomalies during the three El Niño events

From the geographic distribution of SPI values for the 2015/16 event during early summer (Fig. 3a) and late summer (Fig. 3d), the extreme magnitude and extent of the drought are

apparent. Most of southern Africa south of 10°S, including Zimbabwe, much of Botswana, most of Mozambique, Namibia, South Africa and western Zambia, experienced a drastic decrease in the summer rainfall during this event, particularly OND. East Africa experienced above average rainfall during this period, which is a “typical” El Niño response (Ropelewski and Halpert, 1987; Farmer, 1988; Hutchinson, 1992; Hastenrath *et al.*, 1993; Gamoyo *et al.*, 2015). Parts of the interior and east coast of South Africa were particularly negatively impacted during OND 2015 with an SPI value of less than -2. Negative SPI values (indicative of drought) peaked during OND 2015. Over much of the interior and eastern South Africa (Fig. 3a), SPI values of less than -2.5 occurred, with probability of occurrence being 0.006 and therefore can be considered exceptionally intense drought, while southern Zambia, Zimbabwe, Botswana, Lesotho and Swaziland experienced SPI below around -1.7 (probability of 0.04, indicative of extreme drought conditions).

Despite a strong correlation between ENSO and southern African rainfall there are important differences in the space/time structure of rainfall anomalies between the three strong El Niño events (Fig. 3). Firstly, the summer drought as a whole was far more extreme in 2015/16 than either 1982/83 or 1997/98 (see below). In 2015/16 the drought peaked in the early OND season (Figs. 3a vs. 3d), whilst in 1982/83 the seasonal evolution was reversed with stronger and more extensive drought in JFM than in OND (Figs. 3f vs 3c). The 1997/98 event experienced predominantly dry conditions in OND (but not in much of Botswana, Namibia, Mozambique or northeastern South Africa) and mainly average to above average rainfall in JFM.

To put this further into context, Figure 4 illustrates the SPI IAF curves for the three major El Niño events, compared to IAF curves of various benchmark return periods. These IAF curves represent drought intensity at all spatial scales up to the whole southern Africa domain. For

OND the El Niño event of 2015/16 produced by far the most extreme drought within the 116-year historical period and the estimated return period for the SPI-3 IAF curve is 232 years (with a range of 223-250 years) (Fig. 4a). As such, the wider southern Africa region experience drought of unprecedented intensity, leading to pronounced adverse impacts on water resources and agriculture. For the entire ONDJFM 2015/16 rainy season as a whole (see Fig. 4b), the estimated return period of the SPI-6 IAF curve is 79 years (sensitivity range of 73-92 years). In contrast the SPI IAF curves for the El Niño events of 1982/83 and 1997/98 are clearly not extreme. Return periods are less than the minimum retrievable interval of 1 block (30 years). Indeed for 1997/98 the SPI-3 (SPI-6) IAF curve is 'exceeded' in about 40% (50%) of the 116 observed years (not shown), whilst for 1982/83 the figures are 37% (8%).

On a local scale, stations across the South Africa recorded one of the lowest rainfall totals since 1950 during the 2015/16 summer (Fig. 5). In the Free State (Fig. 5c) and the northern KZN coast (Fig. 5d), the lowest summer rainfall total over the entire period was recorded during the 2015/16 summer. Although only a handful of stations are used here to highlight the lack of rainfall, the full SAWS station dataset indicates that 2015 was the driest year on record since 1904 (de Jager, 2016). The severity of the 2015/16 drought is not only linked to that summer but also the prevailing dry conditions from the previous summer. In some cases, the dry conditions extend further back, with station data from the east coast of South Africa (KZN, Figs. 5d-e,) indicating below average rainfall since around 2000/01. The reason for these dry conditions along the east coast of South Africa since 2000/01 is not well understood and is part of on-going research. However, it is well known that there have been decadal periods of drought and flood conditions over many parts of South Africa (Tyson *et al.*, 1975; Reason and Rouault, 2002; Malherbe *et al.*, 2014; Jury, 2015; Reason, 2016). Towards the end of the summer, the southeast coast and northern interior of South Africa did get some

relief with late summer rains. This is evident in the station data, with the Eastern Cape (Fig. 5f) and Gauteng stations (Fig. 5b) not showing as large a decrease in the summer rainfall as that noted elsewhere. Despite the sub-continental wide extent of the 2015/16 drought evident from the SPI, the station data illustrates some important variability in drought intensity both across the six sub-domains, and between stations within. Such local scale variability must be borne in mind in the context of dissemination of seasonal climate predictions.

4. Mechanisms of El Niño teleconnections to southern Africa in 2015/16 compared to previous events

In this section, we analyse the set of processes described in *Section 1* thought to be involved in the teleconnection between ENSO and rainfall over southern Africa. We compare the state of relevant diagnostic fields in 2015/16 with the other two El Niño events to explain some of the marked differences in rainfall between these events.

4.1 Pacific and regional SST anomalies

In terms of Pacific SSTs, the 2015/16 and 1997/98 El Niño peaked slightly earlier than normal, around November, whereas other events, including 1982/83 tend to peak around December/January (Fig. 2). As such the seasonal evolution of rainfall anomalies over southern Africa, described above, is coherent with the timing of peak anomalies in the Pacific. In terms of spatial characteristics, although all El Niño events are associated with warming in the tropical Pacific, different types of El Niños may exist (Ashok *et al.*, 2007; Kao and Yu, 2009; Yeh *et al.*, 2009; Yu and Kim, 2013; Johnson, 2013). The two most recognized types are the Central Pacific (CP), which has the warmer SST anomalies centred around the Date Line, also referred to as the El Niño Modoki, and the more conventional

Eastern-Pacific (EP) or ‘canonical’ El Niño (Rasmusson and Carpenter, 1982) with warm anomalies in the eastern part of the basin (Ashok *et al.*, 2007; Kao and Yu, 2009). Regarding the three sample El Niño events here, 1982/83 and 1997/98 are both EP events while 2015/16 shows both EP and CP characteristics. The strongest warming in 2015/16 is more towards the central Pacific (Fig. 6), such that it satisfies the El Niño Modoki Index (Ashok *et al.*, 2007) definition as a CP El Niño but with strong anomalous warming also present in the eastern Pacific with a larger positive anomaly in Niño-3 Index, indicating that the 2015/16 El Niño would more likely be classified as an EP event.

These two El Niño types are associated with different impacts around the world (Ashok *et al.*, 2007; Weng *et al.*, 2009; Taschetto *et al.*, 2010; Pradhan *et al.*, 2011; Ratnam *et al.*, 2014; Hoell *et al.*, 2015; Preethi *et al.*, 2015). The difference is thought to be due to the influence the location of the warm SST anomaly has on the Walker Circulation, tropical latent heating and resulting large-scale wave structure across the tropical and extra-tropical atmosphere. Within the tropics this is often interpreted using the Matsuno-Gill framework (Matsuno, 1966, Gill, 1980) and we consider the regional expression of such responses over our study domain in *Section 4.3*.

The El Niño teleconnection to southern Africa is further complicated by SST structures in the tropical/subtropical Indian and Atlantic oceans adjacent to southern Africa which are known to influence the circulation and rainfall patterns over southern Africa (Mason, 1995; Reason and Godfred-Spenning, 1998; Goddard and Graham, 1999; Landman and Mason, 1999; Reason 1999; Reason and Mulenga 1999; Reason 2001; Behera and Yamagata, 2001; Reason 2002; Rouault *et al.*, 2003; Reason *et al.*, 2006; Washington and Preston, 2006; Vigaud *et al.*, 2007; Preethi *et al.*, 2015; Hoell *et al.*, 2017). These regional SSTs can be both partially

dependent on the state of ENSO (e.g. Goddard and Graham, 1999; Hoell *et al.*, 2015) and independent of ENSO (e.g. Reason, 2001; Washington and Preston, 2006). There are pronounced differences between the three major El Niño events, most notably; (i) 2015/16 experienced basin-wide warm anomalies in the Indian Ocean, with a local maximum of over 1°C in the extreme west of the basin. There was an absence of the cold anomaly in the mid-latitude Indian and Atlantic oceans at ~40°S characteristic of composite El Niño responses (Reason *et al.*, 2000); (ii) In 1997/98 a pronounced Indian Ocean dipole structure was apparent, responsible for the very strong positive rainfall anomalies across East Africa (Fig. 3b) then (Behara *et al.*, 2005); (iii) 1982/83 exhibited weaker warming in the Indian Ocean. The influence of these different SST patterns on moisture availability and regional circulation in the three El Niño events is discussed in *Section 4.3*.

4.2 Tropical-Extratropical Connections

We consider the state of El Niño influence on the PSA and its interaction with the SAM during our sample of three major El Niño events. The PSA has a strong effect on circulation and rainfall over South America (e.g. Mo and Paegle, 2001) and a discernible effect further ‘downstream’ over the southeast Atlantic / southern Africa (Colberg *et al.*, 2004). However, the specific PSA response, in particular the longitudinal shift, to the different types of ENSO events, is not completely understood. Some authors have suggested that the longitudinal movement of the PSA pattern could be linked to the associated tropical SST anomalies (e.g. Sun *et al.*, 2013; Wilson *et al.*, 2014), whereas others suggest that the pattern is relatively stationary (e.g. Liu and Alexander, 2007; Ding *et al.*, 2012). The development of the anomalous wave patterns from the more typical PSA pattern have previously been linked to atypical El Niño conditions over southern Africa (e.g. Lyon and Mason, 2007).

In all three sample El Niño events analysed here, PSA patterns are evident but with the centre of the anomalies shifted in each event. The typical PSA pattern during EP El Niño events contains, over the Southern Ocean, a positive anomaly centred over the eastern South Pacific sector (around 120°W), with negative anomalies positioned on either side of it. During OND 2015/ (Fig. 7a), the negative height anomalies south and southwest of New Zealand are shifted polewards compared to the composite (Fig. 7d), while the positive anomaly west of the Drake Passage is positioned further equatorwards. During OND 1997, an eastward shift in the centre of the positive height anomaly (centred around 90°W near Drake Passage) in the South Pacific sector took place (Fig. 7b) and it remained there into the late summer (Fig. 8b). OND 1982 showed a similar anomaly pattern to that of the composite (Fig. 7c), however a slight westward shift in the centre of the PSA anomalies is found in JFM 1983 (Fig. 8c).

A key aspect with these PSA shifts is likely the downstream effects over the South Atlantic towards Africa. Typically during El Niño, the PSA leads to a stronger and eastward shift in the subtropical South Atlantic High Pressure (Colberg *et al.*, 2004). In OND 2015, a positive anomaly to the east of South America (around 30°S, 40°W) was considerably stronger than what is typically found in El Niño events. This feature is part of a stronger high pressure anomaly extending right across the tropical Atlantic, the Angola Low region and all of southern Africa. Furthermore, Lyon and Mason (2007) demonstrate that a similar, but negative, anomaly positioned slightly further south (40°S), as part of an anomalous wave train across the South Atlantic, could account for the stronger Angola Low experienced in 1997/98.

The negative height anomaly present over the whole of Antarctica during JFM 2016 (Fig. 8a) contains similarities to a positive phase in the SAM (Hartman and Lo, 1998; Thompson and

Wallace, 2000), typically associated with anomalously wet summers over southern Africa (Gillett *et al.*, 2006). As alluded to earlier, the rationale behind the connection between ENSO and SAM is that anomalous heating in the tropics strengthens the meridional temperature gradient thereby enhancing the subtropical jets, which act as waveguides to steer transient eddies on a more equatorward and zonal path (Seager *et al.*, 2003; L'Heureuz and Thompson, 2006). Fogt *et al.*, (2011) find that certain combinations of SAM and ENSO phases can lead to a weakening (strengthening) of the high-latitude ENSO signal due to opposing (reinforcing) transient eddy momentum fluxes. This may lead to amplifying the resulting circulation anomalies and maintains the ENSO teleconnection. In particular, these authors note that when El Niño occurs with negative SAM or La Niña with positive SAM, the anomalous transient eddy fluxes act to reinforce each other in way that amplifies the resulting circulation anomalies and maintains the ENSO teleconnection. This implies that positive SAM and El Niño in 2015/16 (Fig. 8a) could have led to the weakening of the ENSO signal across southern Africa, resulting in JFM not being as dry as that experienced during OND. Similarly, the negative SAM in 1982/83 (Fig. 7c) reinforces the ENSO signal, leading to the typical dry conditions experienced throughout the summer. However, modelling experiments would be required to examine this hypothesis of an in/out phase relationship between SAM and PSA and its impacts on southern Africa, which are beyond the scope of this study.

4.3 Regional Circulation Anomalies

The state of the dominant controls on moisture flux and convergence across southern Africa and the SIOCZ, specifically the Angola Low and the South Indian Ocean High is now examined. El Niño is typically associated with positive geopotential height anomalies throughout the tropics which includes the Angola Low. The events of 2015/16 and 1982/83 are broadly consistent with this (Figs. 9 and 10) resulting in a weaker Angolan Low, most

notably in JFM especially in 1982/83 (Figs. 9b and 10f). In contrast, the 1997/98 El Niño reveals an uncharacteristic negative anomaly in geopotential height in the Angola / Namibia region (Figs. 9a and 10b, 10e) with a centre displaced westward of the climatological centre of the low. This unusually strong Angola Low in 1997/98 is thought to have resulted in the atypical precipitation response to El Niño conditions experienced in the region that summer through enhanced moisture transport from the tropical African continent and tropical eastern Atlantic Ocean (Reason and Jagadheesha, 2005; Lyon and Mason, 2007) (Fig. 10b). The importance of the moisture from the tropical southeast Atlantic for the Angola Low and summer rainfall has been highlighted by Cook *et al.*, (2004).

The excess moisture found over tropical Africa in 1997/98 was due to a combination of the strong increase in the eastward moisture flux around the enhanced Angola Low and a westward flux from the anomalously warm equatorial warmer tropical Indian Ocean (Fig. 10b), leading to an increase in the rainfall in eastern Africa then (Lyon and Mason, 2007). The presence of a strong anticyclonic anomaly that typically develops over the tropical Indian Ocean during an El Niño event (as described earlier) led to this increased eastward moisture flux in 1997/98 (not shown). This anticyclonic anomaly was not as pronounced in 2015/16 as in 1997/98 (not shown). Furthermore, although anomalously warm SSTs were present over much of the tropical Indian Ocean in 2015/16 (Fig. 6a), the strong anticyclonic anomaly over western southern Africa and extending into central Africa (Fig. 10a) led to southwesterly moisture flux anomalies over Tanzania and northern Mozambique and hence, less moisture transport from the Indian Ocean into southern Africa than average. This strong anticyclonic anomaly in OND 2015 is not evident in the other two events, but is present in JFM in 1983 (Fig. 10f). In the case of OND 1982, a cyclonic anomaly in the Mozambique Channel (Fig.

10c) also led to southwesterly moisture flux anomaly over northern Mozambique and hence less moisture transport into the mainland from the Indian Ocean.

It was not only the reduced moisture from the tropical Indian Ocean that likely led to the drier conditions experienced over southern Africa during 2015/16. Another key moisture source for the region is the southwest Indian Ocean, particularly during JFM (D'Abreton and Tyson, 1995). During 2015/16, eastward moisture flux into southern Mozambique, northern South Africa and southern Zimbabwe is only marginally reduced in OND (Fig. 10a), but the reduction is more pronounced in JFM (Fig. 10d). This low level moisture flux anomaly could be indicative of a weakening of the onshore moisture transport and the SIOCZ being shifted to the northeast of Madagascar. The shift in the SIOCZ and associated dry conditions over the continent often happens during El Niño (Cook, 2001; Manhique *et al.*, 2011; Ratnam *et al.*, 2014). On the other hand, OND 1997 shows a substantial increase in moisture originating from the Zambia/Angola region (Fig. 10b), due to a stronger Angola Low which, as discussed earlier, is enhanced during the late summer (Fig. 10e), and strong easterly anomalies over the tropical west Indian Ocean.

At the 500 hPa level, similar anomalous geopotential height patterns to that found at the 850 hPa level are present in each event. It is important to also consider mid-levels as well as 850 hPa since, regionally, the Botswana High exerts a strong influence on southern African rainfall (Matarira, 1990; Reason, 2016; Driver and Reason, 2017). Typically during OND, the positive geopotential height anomalies found during El Niño events are generally not as pronounced as that during JFM. However, this is not the case with 2015/16, which contains a strong positive anomaly positioned over southern Africa during OND (Fig. 11a), indicating a strong Botswana High. The impact of this anomalous high pressure pattern is through

stronger subsidence in the mid- to upper levels over southern Africa (Fig. 12b). This subsidence results in unfavourable conditions for rainfall and in conjunction with less moisture transport into the region was likely responsible for the very dry OND 2015 (see Fig. 3a).

There is little evidence to suggest a similar response (stronger Botswana High) during OND 1997 or 1982 (Figs. 11b and 11c, respectively). However, anomalous downward motion was still present in the mid- to upper levels in OND 1982 (Fig. 12d), which became considerably stronger in JFM (Fig. 12h). This stronger downward motion in JFM 1983 is likely associated with the presence of a stronger Botswana High during this period (Fig. 13c). Furthermore, the negative 500 hPa geopotential height anomaly to the south of the continent during JFM 1982/83 (Fig. 13c) is also expected to have influenced the stability of the atmosphere over southern Africa through transporting cool, dry South Atlantic air over the landmass. A similar positioned feature, non-ENSO related, has been linked to dry conditions experienced over southern Africa in 1967/68 (Mulenga *et al.*, 2003). The position of this negative anomaly, a weaker Angola Low and the stronger Botswana High are consistent with the drier conditions experienced during JFM 1983 (Fig. 3f). The development or maintenance of such anomalies is likely linked to the teleconnection of ENSO into the extra-tropics, as described earlier.

5. Discussion and Summary

The austral summer wet season of 2015/16 over southern Africa was exceptionally dry. During the early summer (OND) in particular, SPI values of <-2 (exceptionally intense drought) were observed across extensive areas of South Africa in particular. Over the sub-continent as a whole this OND event was the driest in the historical record with an estimated return period of more than 200 years. Locally, station data from South Africa indicated that it

may have been the driest summer for some parts of the country since 1950 (the start date of the data used). In fact, the South African Weather Service claimed that it was part of the driest year (2015) in South Africa since the early 1900s. These very dry conditions are associated with the strong El Niño event taking place in the Pacific at the same time. The negative impacts of the 2015/16 event were likely compounded by the dry conditions experienced during the previous summer season. The reasons behind the dry 2014/15 summer are not included in the analysis, but is conceivable that the weak El Niño event during that period may have played a role.

This early summer drought in OND 2015 is in contrast to previous El Niño events, which typically have drier conditions in JFM (e.g. 1982/83 El Niño event). The timing of the driest period within the summer in both 1982/83 and 2015/16 corresponds to when SST anomalies in the Pacific were reaching their peak. However, there are also summers where a strong El Niño event is associated with average to above average rainfall in southern Africa, such as the strong 1997/98 El Niño event. These contrasting rainfall patterns highlight the non-linear relationship between El Niño and southern African climate, which has been well documented (Reason and Jagadheesha, 2005; Fauchereau *et al.*, 2009; Boulard *et al.*, 2013). It also highlights the need for a better understanding of how El Niño influences regional rainfall because a drought warning is typically issued by meteorological agencies in southern Africa during the onset of an El Niño event sometime in the previous austral winter or spring. However, as shown here, such drought outcomes do not always evolve in a coherent form. In addition, there are intra-seasonal characteristics in the rainfall that need to be considered.

In this study, emphasis is placed on the regional circulation anomalies over and surrounding Africa, associated with three strong El Niño events. Although each event is unique, there are

a few key regional circulation features that play an important role in producing unfavourable conditions for rainfall when they are either weakened / intensified; namely, the Angola Low, Botswana High and the subtropical SIHP. It is mostly a combination of the anomalous circulation associated with these features that results in the unfavourable rainfall conditions during El Niño, through reducing the moisture transport into the continent or suppressing convection via enhanced subsidence. However, it is evident that changes in one regional circulation system can dominant a particular summer or even at different times during the season. This was particularly the case for 2015/16, with the mid-levels over southern Africa being dominated by a much stronger Botswana High in OND than that experienced in the other events.

Other factors influencing rainfall pattern in 2015/16 include weaker anticyclonic circulation around the SIHP, resulting in less moisture being transported into the continent from the subtropical South Indian Ocean. There is some evidence to suggest a weaker Angola Low in OND 2015, but it is not that distinct compared to the weaker Angola Low in JFM 2016 or to that seen in other El Niño events. Instead, a strong low level anticyclonic anomaly extending across western and central southern Africa in 2015/16 led to southwesterly moisture flux anomalies over Tanzania and northern Mozambique, reducing the amount of moisture entering the continent from the tropical Indian Ocean.

The 1982/83 event has some similarities to 2015/16, such as the weaker moisture transport from the subtropical South Indian Ocean into southern Africa. During these two El Niño events, moisture convergence appears to have taken place over the northern parts of Madagascar and western Indian Ocean, resembling a northward shift in the SIOCZ. Large areas of northern and eastern Madagascar received above average rainfall during 1982/83 and

2015/16. The shift in the SIOCZ and associated dry conditions over the continent is common occurrence during El Niño events (Cook, 2001; Manhique *et al.*, 2011; Ratnam *et al.*, 2014). More importantly, the key role of the weaker Angola Low and stronger Botswana High was again evident in 1982/83, with the driest part of that summer (JFM) occurring when these two features were particularly weak/strong, respectively.

Of the three events, the regional circulation anomalies during 1997/98 were the most uncharacteristic to that of past El Niño events. Although there was a decrease in the moisture sourced from the subtropical South Indian Ocean during 1997/98, the anomalously strong Angola Low continued to advect moisture from the southeast tropical Atlantic Ocean and the continental interior throughout the late summer months. There was also enhanced moisture flux from the tropical Indian Ocean which led to more rainfall experienced over southern Africa than that which typically takes place during El Niño (Reason and Jagadheesha, 2005; Lyon and Mason, 2007). There was also very little evidence of any change in the Botswana High in 1997/98.

On the planetary-scale, the PSA pattern was present during OND 2016, with subtle differences in the location of the anomaly centres from the composite El Niño pattern. The difference in the location of the anomaly centres might be attributed to the warming in the tropical Pacific being more central to that of more typical eastern Pacific El Niño events. Typically during El Niño, the PSA leads to a stronger and eastward shifted South Atlantic High Pressure (Colberg *et al.*, 2004), which is unfavourable for a strong Angola Low and cloudband development. However, in some events, such as 1997/98, the development of the anomalous wave patterns from the more typical PSA pattern produces atypical El Niño conditions over southern Africa through enhancing the Angola Low (Lyon and Mason, 2007).

599 In the case of 2015/16, the anomalous wave activity, potentially excited from the relatively
600 early warming in tropical Pacific SSTs and associated convection, may have assisted in
601 generating and maintaining the strong anomalous anticyclonic circulation (stronger Botswana
602 High) in the mid- to upper levels over southern Africa during the early summer. JFM 2016
603 revealed a slightly different pattern in the upper levels in the mid- to high latitudes, with the
604 presence of positive SAM type pattern and a weaker PSA. As noted by Fogt *et al.*, (2011),
605 such modes coupled with ENSO can act to reinforce or oppose the signal from the tropics. In
606 this case, the out of phase relationship during JFM 2016 could account for this period not
607 being as dry as that experienced during the early summer.

608

609 ENSO is the mode of variability that has the greatest impact on subtropical southern Africa
610 during the austral summer, the season when the region receives most of its rainfall. However,
611 the underlying atmospheric circulation patterns during each El Niño event that control rainfall
612 variability in the region are still not completely understood. It is also not obvious to what
613 extent SST anomalies in the neighbouring oceans act independently from ENSO or to what
614 extent they combine to influence regional circulation patterns and local rainfall patterns. The
615 lack of clarity is of concern considering how dependent the region is on summer rainfall.
616 Results here highlight that in each strong event, key regional scale circulation patterns,
617 influenced by planetary scale processes, have an impact on the spatial and temporal evolution
618 of the summer rainfall. Thus, the findings advocate the need for added research into these
619 regional circulation features for seasonal forecasting and long-term climate projections for
620 southern Africa.

1 **Acknowledgements:**

2 NCEP Reanalysis 2, GPCC Precipitation data and the OISST data were provided by the
3 NOAA/OAR/ESRL PSD, Boulder, Colorado, from <http://www.esrl.noaa.gov/psd/>. We thank
4 the South African Weather Service (SAWS) for providing the station data. We would also
5 like to thank the reviewers for their insightful comments that helped improve the manuscript.
6 This work was supported by the Natural Environment Research Council (NERC) Future
7 Climate For Africa (FCFA) regional consortium project 'UMFULA' (NE/M020258 and
8 NE/M020223/1).

Peer Review Only

References:

- Ashok, K., Behera, S.K., Rao, S.A., Weng, H., & Yamagata, T. (2007). El Niño Modoki and its possible teleconnection. *J. Geophys. Res.* **112**: C11007, doi:10.1029/2006JC003798
- Behera, S.K., & Yamagata, T. (2001). Subtropical SST dipole events in the southern Indian Ocean. *Geophys. Res. Lett.* **28**: 327-330.
- Behera, S.K., Luo, J.-J., Masson, S., Delecluse, P., Gualdi, S., Navarra, A., & Yamagata, T. (2005). Paramount impact of the Indian Ocean dipole on the East African short rains: A CGCM study. *J. Clim.* **18**: 4514–4530
- Bosilovich, M.G., Chen, J., Robertson, F.R., & Adler, R.F. (2008). Evaluation of global precipitation in reanalyses. *J. Appl. Meteorol. Climatol.* **47**(9), 2279-2299.
- Boulard, D., Pohl, B., Crétat, J., Vigaud, N., & Pham-Xuan, T. (2013). Downscaling large-scale climate variability using a regional climate model: the case of ENSO over Southern Africa. *Clim. Dyn.* **40**: 1141-1168.
- Bromwich, D.H., Fogt, R.L., Hodges, K.I., & Walsh, J.E. (2007). A tropospheric assessment of the ERA-40, NCEP, and JRA-25 global reanalyses in the polar regions. *J. Geophys. Res.* doi:10.1029/2006JD007859
- Cai, W.J., & Watterson, I.G. (2002). Modes of interannual variability of the Southern Hemisphere circulation simulated by the CSIRO climate model. *J. Clim.* **15**: 1159-1174.
- Cai, W., Sullivan, A., & Cowan, T. (2011). Interactions of ENSO, the IOD, and the SAM in CMIP3 Models. *J. Clim.* **24**: 1688–1704
- Calow, R.C., Macdonald, A.M., Nicol, A.L., & Robins, N.S. (2010). Ground water security and drought in Africa: linking availability, access, and demand. *Gr. Water.* **48**(2): 246-256.

- 1 Carvalho, L.M.V, Jones, C., & Ambrizzi, T. (2005). Opposite phases of the Antarctic
2 Oscillation and relationships with intraseasonal to interannual activity in the tropics during
3 the austral summer. *J. Clim.* **18**: 702-718.
4
- 5 Colberg, F., Reason, C.J.C., & Rodgers, K. (2004). South Atlantic response to El Niño–
6 Southern Oscillation induced climate variability in an ocean general circulation model. *J.*
7 *Geophys. Res.* **109**: C12015, doi:10.1029/2004JC002301
8
- 9 Coles, S., Bawa, J., Trenner, L., & Dorazio, P. (2001). An introduction to statistical modeling
10 of extreme values (Vol. 208). London: Springer.
11
- 12 Cook K.H. (2000). The South Indian Convergence Zone and Interannual Rainfall Variability
13 over Southern Africa. *J. Clim.* **13**: 3789-3804.
14
- 15 Cook, K.H. (2001). A Southern Hemisphere Wave Response to ENSO with Implications for
16 Southern Africa Precipitation. *J. Atmos. Sci.* **58**: 2146-2162.
17
- 18 Cook, C., Reason, C.J.C, & Hewitson, B.C. (2004). Wet and dry spells within particularly
19 wet and dry summers in the South African summer rainfall region. *Climate Res.* **26**: 17-31.
20
- 21 D’Abreton, P.C, & Lindesay, J.A. (1995). Divergent and non-divergent water vapour
22 transport over southern Africa during wet and dry conditions. *Meteor. Atmos. Phys.* **55**: 297-
23 306.
24
- 25 de Jager, E. (2016). South Africa - Annual Total Rainfall. *South African Weather Services*.
26 [Online] Available at:
27 [http://www.weathersa.co.za/images/documents/299/CLS-CI-GEN-INFO-](http://www.weathersa.co.za/images/documents/299/CLS-CI-GEN-INFO-109%201%20SA%20Annual%20Total%20Rainfall.pdf)
28 [109%201%20SA%20Annual%20Total%20Rainfall.pdf](http://www.weathersa.co.za/images/documents/299/CLS-CI-GEN-INFO-109%201%20SA%20Annual%20Total%20Rainfall.pdf).
29
- 30 Ding, Q., Steig, E.J., & Wallace, J.M. (2012). Influence of the tropics on the southern annular
31 mode. *J. Clim.* **25**: 6330-6348.
32

- 1 Driver, P., & Reason, C.J.C. (2017). Variability in the Botswana High and its relationships
2 with rainfall and temperature characteristics over southern Africa. *Int. J. Climatol.* doi:
3 10.1002/joc.5022
4
- 5 Farmer, G. (1988). Seasonal forecasting of the Kenya Coast short rains 1901–84. *Int. J.*
6 *Climatol.* **8**: 489-497.
7
- 8 Fauchereau, N., Pohl, B., Reason, C.J.C, Rouault, M., & Richard, Y. (2009). Recurrent daily
9 OLR patterns in the Southern Africa/Southwest Indian Ocean region, implications for South
10 African rainfall and teleconnections. *Clim. Dyn.* **32**: 575-591.
11
- 12 Fogt, R.L., & Bromwich, D.H. (2006). Decadal variability of the ENSO teleconnection to the
13 high-latitude South Pacific governed by coupling with the southern annular mode. *J. Clim.*
14 **19**: 979-997.
15
- 16 Fogt, R.L., Bromwich, D.H., & Hines, K.M. (2011). Understanding the SAM influence on
17 the South Pacific ENSO teleconnection. *Clim. Dyn.* **36**: 1555-1576, doi:10.1007/s00382-010-
18 0905-0
19
- 20 Gamoyo, M., Reason, C. & Obura, D. (2015), Rainfall variability over the East African coast,
21 *Theor. Appl. Climatol.*, **120** (1-2), 311–322.
22
- 23 Ghil, M., & Mo, K. (1991). Intraseasonal oscillations in the global atmosphere. Part I:
24 Northern Hemisphere and tropics. *J. Atmos. Sci.* **48**: 752-779.
25
- 26 Gill, A.E. (1980). Some simple solutions for heat-induced tropical circulation. *Quart. J. Roy.*
27 *Meteor. Soc.* **106**: 447–462, doi:10.1002/qj.49710644905.
28
- 29 Gillett, N.P., Kell, T.D., & Jones, P.D. (2006). Regional climate impacts of the Southern
30 Annular Mode. *Geophys. Res. Lett.* **33**: L23704, doi:10.1029/2006GL027721
31
- 32 Goddard, L., & Graham, N.E. (1999). Importance of the Indian Ocean for simulating rainfall
33 anomalies over eastern and southern Africa. *J. Geophys. Res.* **104**: 19099–19116
34

- 1 Harrison, M.S.J. (1984). A generalized classification of South African rain-bearing synoptic
2 systems. *Int. J. Climatol.* **4**: 547-560.
3
- 4 Hart, N.C.G., Reason, C.J.C., & Fauchereau, N. (2010). Tropical–Extratropical Interactions
5 over Southern Africa: Three Cases of Heavy Summer Season Rainfall. *Mon. Wea. Rev.*
6 **138**(7): 2608-2623.
7
- 8 Hart, N.C.G., Reason, C.J.C., & Fauchereau, N. (2013). Cloud bands over southern Africa:
9 Seasonality, contribution to rainfall variability and modulation by the MJO. *Clim Dyn.* **41**:
10 1199-1212.
11
- 12 Hartmann, D.L., & Lo, F. (1998). Wave-driven Zonal flow vacillation in the Southern
13 Hemisphere, *J. Atmos. Sci.* **55**: 1303-1315.
14
- 15 Hastenrath, S., Nicklis, A., Greischar, L. (1993). Atmospheric-hydrospheric mechanisms of
16 climate anomalies in the western equatorial Indian Ocean. *J. Geophys. Res.* **98**: 20219-
17 20235.
18
- 19 Hoell, A., Funk, C., Magadzire, T., Zinke, J., & Husak, G. (2015). El Niño-Southern
20 Oscillation diversity and Southern Africa teleconnections during Austral Summer. *Clim. Dyn.*
21 **45**: 1583–1599.
22
- 23 Hoell, A., Funk, C., Zinke, J., & Harrison, L. (2017). Modulation of the Southern Africa
24 precipitation response to the El Niño Southern Oscillation by the subtropical Indian Ocean
25 Dipole. *Clim Dyn.* **48**(7): 2529–2540.
26
- 27 Hutchinson, P. (1992). The Southern Oscillation and prediction of ‘Der’ season rainfall in
28 Somalia. *J. Clim.* **5**: 525-531.
29
- 30 Jin, D., & Kirtman, B.P. (2009). Why the Southern Hemisphere ENSO responses lead ENSO.
31 *J. Geophys. Res.* **114**: D23101, doi:10.1029/2009JD012657.
32
- 33 Johnson, N.C. (2013). How many ENSO flavors can we distinguish? *J. Clim.* **26**: 4816-4827
34

- 1 Jury, M.R. (2015). Factors contributing to a decadal oscillation in South African rainfall.
2 Theor. Appl. Climatol., **120**: 227–237
3
- 4 Kao, H-Y., & Yu, J-Y. (2009). Contrasting eastern-Pacific and central- Pacific types of
5 ENSO. *J. Clim.* **22**: 615-632.
6
- 7 Karoly, D.J. (1989). Southern Hemisphere circulation features associated with El Niño–
8 Southern Oscillation events. *J. Clim.* **2**: 1239-1252.
9
- 10 Kidson, J.W. (1988). Interannual variations in the Southern Hemisphere circulation, *J. Clim.*
11 **1**: 1177-1198.
12
- 13 Kanamitsu, M., Ebisuzaki, W., Woollen, J., Yang, S.K, Hnilo, J., Fiorino, M., & Potter, G.L.
14 (2002). NCEP-DOE AMIP II Re-Analysis (R-2). *Bull. Amer. Meteor. Soc.* **83**: 1631-1643.
15
- 16 Landman, W., & Mason, S. (1999). Change in association between Indian Ocean sea-surface
17 temperatures and summer rainfall over South Africa and Namibia. *Int. J. Climatol.* **19**: 1477-
18 1492.
19
- 20 Lazenby, M.J., Todd, M.C., & Wang, Y. (2016), Climate model simulation of the South
21 Indian Ocean Convergence Zone: mean state and variability. *Climate Research*, **68**, 59-71.
22
- 23 Lindesay, J.A. (1988). Southern African rainfall, the Southern Oscillation and a Southern
24 Hemisphere semi-annual cycle. *J. Climatol.* **8**: 17-30.
25
- 26 Liu, Z., & Alexander, M. (2007). Atmospheric bridge, oceanic tunnel, and global climatic
27 teleconnections. *Rev. Geophys*, **45**: RG2005, doi:10.1029/2005RG000172.
28
- 29 L’Heureux, M.L., & Thompson, D.W.J. (2006). Observed relationships between the El Niño–
30 Southern Oscillation and the extratropical zonal-mean circulation. *J. Clim.* **19**: 276-287.
31
- 32 Lyon, B., & Mason, S.J. (2007). The 1997-98 summer rainfall season in southern Africa. Part
33 I: Observations. *J. Clim.* **20**: 5134-5148,

- 1
2 Matsuno, T. (1966). Quasi-geostrophic motions in the equatorial area. *J. Meteor. Soc. Japan*.
3 **44**: 25-43.
4
- 5 Malherbe, J.A., Landman, W.A., & Engelbrecht, F.A. (2014). The bi-decadal rainfall cycle,
6 Southern Annular Mode and tropical cyclones over the Limpopo River basin, southern
7 Africa. *Clim. Dyn.* **42**: 3121-3138.
8
- 9 Manhique, A.J., Reason, C.J.C., Rydberg, L., & Fauchereau, N. (2011). ENSO and Indian
10 Ocean sea surface temperatures and their relationships with tropical temperate troughs over
11 Mozambique and the Southwest Indian Ocean. *Int. J. Climatol.* **31**: 1-13.
12
- 13 Mason, S. (1995). Sea-surface temperature-South African rainfall associations, 1910-1989.
14 *Int. J. Climatol.* **15**: 119-135.
15
- 16 Matarira, C.H. (1990). Drought over Zimbabwe in a regional and global context, *Int. J.*
17 *Climatol.*, **10**, 609-625
18
- 19 McKee, T.B., Doesken, N.J., & Kleist, J. (1993). The relationship of drought frequency and
20 duration to time scales. In: Proceedings of the Eighth Conference on Applied Climatology,
21 Anaheim, California, 17-22 January 1993. Boston, American Meteorological Society, 179-
22 184.
23
- 24 McPhaden, M.J., Zebiak, S.E., & Glantz, M.H. (2006). ENSO as an integrating concept in
25 earth science. *Science*. **314**: 1739-1745.
26
- 27 Mishra, V., & Cherkauer, K.A. (2010). Retrospective droughts in the crop growing season:
28 Implications to corn and soybean yield in the Midwestern United States, *Agric. For.*
29 *Meteorol.* **150(7)**: 1030-1045.
30
- 31 Mishra, A.K., & Singh, V.P. (2009). Analysis of drought severity-area-frequency curves
32 using a general circulation model and scenario uncertainty. *J. Geophys. Res.*, **114**: D06120,
33 doi:10.1029/2008JD010986
34

- 1 Mitchell, D., AchutaRao, K., Allen, M., Bethke, I., Beyerle, U., Ciavarella, A., ... Zaaboul,
2 R. (2017). Half a degree additional warming, prognosis and projected impacts (HAPPI):
3 background and experimental design. *Geosci. Model Dev.*, **10**(2): 571-583,
4 <https://doi.org/10.5194/gmd-10-571-2017>
5
- 6 Mo, K.C. (2000). Relationships between low-frequency variability in the Southern
7 Hemisphere and sea surface temperature anomalies. *J. Clim.* **13**: 3599-3610.
8
- 9 Mo, K.C., & Higgins, R.W. (1998). The Pacific–South American modes and tropical
10 convection during the Southern Hemisphere winter. *Mon. Wea. Rev.* **126**: 1581-1596.
11
- 12 Mo, K.C., & Paegle, J.N. (2001). The Pacific–South American modes and their downstream
13 effects. *Int. J. Climatol.* **21**: 1211–1229
14
- 15 Moalafhi, B.D., Evans, J.P., & Sharma, A. (2016). Evaluating global reanalysis datasets for
16 provision of boundary conditions in regional climate modelling. *Clim. Dyn.* doi
17 10.1007/s00382-016-2994-x
18
- 19 Mulenga, H.M., Rouault, M., & Reason, C.J.C. (2003). Dry summers over northeastern South
20 Africa and associated circulation anomalies, *Climate Res.* **25**: 29-41.
21
- 22 Munday, C., & Washington, R. (2017). Circulation controls on southern African precipitation
23 in coupled models: The role of the Angola Low. *J. Geophys. Res. Atmos.* **122**: 861-877
24
- 25 Prabhu, A., Kripalani, R.H., Preethi, B., & Pandithurai, G. (2016). Potential role of the
26 February–March Southern Annular Mode on the Indian summer monsoon rainfall: a new
27 perspective. *Clim. Dyn.* **47**:1161–1179
28
- 29 Prabhu, A., Kripalani, R.H., Oh, J., & Preethi, B. (2017). Can the Southern Annular mode
30 influence the Korean summer monsoon rainfall? *Asia-Pac. J. Atmospheric Sci.*, **53**: 217-228,
31 DOI: 10.1007/s13143-017-0029-0.
32

- 1 Pradhan, P.K., Preethi, B., Ashok, K., Krishnan, R., & Sahai, A.K. (2011). Modoki, IOD and
2 Western North Pacific typhoons: Possible implications for extreme events. *J. Geophys. Res.*
3 **116**, D18108, DOI:10.1029/2011JD015666.
- 4
- 5 Preethi, B., Sabin, T.B., Adedoyin, J.A., & Ashok, K. (2015). Impacts of the ENSO Modoki
6 and other tropical Indo-Pacific climate- drivers on African rainfall. *Sci. Rep.*, **5**:16653,
7 DOI:10.1038/srep16653.
- 8
- 9 Rasmusson, E.M., & Carpenter, T.H. (1982). Variations in tropical sea surface temperature
10 and surface wind fields associated with the Southern Oscillation/El Niño. *Mon. Wea. Rev.*
11 **110**: 354-384.
- 12
- 13 Ratnam, J.V., Behera, S.K., Masumoto, Y., & Yamagata T. (2014). Remote effects of El Niño
14 and Modoki events on the austral summer precipitation of Southern Africa. *J. Clim.* **27**: 3802-
15 3815
- 16
- 17 Reason, C.J.C. (1999). Interannual warm and cool events in the subtropical/mid-latitude
18 South Indian Ocean region. *Geophys. Res. Lett.* **26**: 215-218.
- 19
- 20 Reason, C.J.C. (2001). Subtropical Indian Ocean SST dipole events and southern African
21 rainfall. *Geophys. Res. Lett.* **28**: 2225-2227.
- 22
- 23 Reason, C.J.C. (2002). Sensitivity of the Southern African circulation to dipole Sea-Surface
24 Temperature patterns in the South Indian Ocean. *Int. J. Climatol.* **22**: 377-393.
- 25
- 26 Reason, C.J.C. (2016). The Bolivian, Botswana and Bilybara Highs and Southern
27 Hemisphere drought/floods. *Geophys. Res. Lett.* **43**: 1280-1286, doi: 10.1002/2015GL067228
- 28
- 29 Reason, C.J.C, & Godfred-Spenning, C.R. (1998). SST variability in the South Indian Ocean
30 and associated circulation and rainfall patterns over southern Africa. *Meteor. Atmos. Phys.*
31 **66**: 243-258.
- 32
- 33 Reason, C.J.C, & Mulenga, H.M. (1999). Relationship between South African rainfall and
34 SST anomalies in the southwest Indian Ocean. *Int. J. Climatol.* **19**: 1652-1673.

- 1
2 Reason, C.J.C., & Rouault, M. (2002). ENSO-like decadal patterns and South African
3 rainfall. *Geophys. Res. Lett.* **29(13)**: 1638, doi:10.1029/2002GL014663.
4
5 Reason, C.J.C., & Jagadheesha, D. (2005). A model investigation of recent ENSO impacts
6 over southern Africa. *Meteor. Atmos. Phys.* **89**: 181-205.
7
8 Reason, C.J.C., & Rouault, M. (2005). Links between the Antarctic Oscillation and winter
9 rainfall over western South Africa. *Geophys. Res. Lett.* **32**: L07705,
10 doi:10.1029/2005GL022419.
11
12 Reason, C.J.C., Hachigonta, S., & Phaladi, R.F. (2005). Interannual variability in rainy
13 season characteristics over the Limpopo region of southern Africa. *Int. J. Climatol.* **25**: 1835-
14 1853.
15
16 Reason, C.J.C., Landman, W., & Tennant, W. (2006). Seasonal to Decadal Prediction of
17 Southern African Climate and its Links with Variability of the Atlantic Ocean, *Bull. Amer.*
18 *Meteor. Soc.* **87**: 941-955.
19
20 Reason, C.J.C., Allan, R.J., Lindesay, J.A., & Ansell, T.J. (2000). ENSO and climatic signals
21 across the Indian Ocean Basin in the global context: Part I, interannual composite patterns.
22 *Int. J. Climatol.* **20**: 1285-1327.
23
24 Reynolds, R.W., Rayner, N.A., Smith, T.M., Stokes, D.C., & Wang, W. (2002). An improved
25 in situ and satellite SST analysis for climate. *J. Clim.* **15**: 1609-1625.
26
27 Richard, Y., & Pocard, I. (1998). A statistical study of NDVI sensitivity to seasonal and
28 interannual rainfall variations in Southern Africa. *Int. Rem. Sens.* **19(15)**: 2907-2920.
29
30 Rienecker, M.M., Suarez, M.J., Gelaro, R., Todling, R., Bacmeister, J., Liu, E., ... Woollen J.
31 (2011). MERRA: NASA's modern-era retrospective analysis for research and applications. *J.*
32 *Clim.* **24**, 3624–3648.
33

- 1 Robeson, S.M. (2015). Revisiting the recent California drought as an extreme value.
2 *Geophys. Res. Lett.*, 42, doi:10.1002/ 2015GL064593.
3
- 4 Rocha, A., & Simmonds, I. (1997). Interannual variability of south-eastern African summer
5 rainfall. Part 1: Relationships with air-sea interaction processes. *Int. J. Climatol.* **17**: 235-265.
6
- 7 Ropelewski, C.F., & Halpert, M.S. (1987). Global and regional precipitation patterns
8 associated with El Niño/southern oscillation. *Mon. Wea. Rev.* **115**: 1606-1626.
9
- 10 Rouault, M., & Richard, Y. (2003). Intensity and spatial extension of drought in South Africa
11 at different time scales. *WaterSA.* **29**(4): 489-500.
12
- 13 Rouault, M., Florenchie, P., Fauchereau, N., & Reason, C.J.C. (2003). South east tropical
14 Atlantic warm events and southern African rainfall. *Geophys. Res. Lett.* **30**: 8009-8013.
15
- 16 SADC. (2016a). SADC regional situation update on El Nino-induced drought, 2016. Issue
17 02, 12th September 2016.
18 [https://www.sadc.int/files/9514/7403/9132/SADC_Regional_Situation_Update_No-2_16-09-](https://www.sadc.int/files/9514/7403/9132/SADC_Regional_Situation_Update_No-2_16-09-2016.pdf)
19 [2016.pdf](https://www.sadc.int/files/9514/7403/9132/SADC_Regional_Situation_Update_No-2_16-09-2016.pdf) accessed 30/12/17
20
- 21 SADC. (2016b). SADC Regional Vulnerability Assessment and Analysis Synthesis Report
22 2016: *State of Food Insecurity and Vulnerability in the Southern African Development*
23 *Community*, 66pp.
24
- 25 Saji, N.H., Goswami, B.N., Vinayachandran, P.N., & Yamagata, T. (1999). A dipole in the
26 tropical Indian Ocean. *Nature.* **401**: 360–363.
27
- 28 Schneider, D.P., Okumura, Y., & Deser, C. (2012). Observed Antarctic Interannual Climate
29 Variability and Tropical Linkages. *J. Clim.* **25**: 4048-4066.
30
- 31 Schneider, U., Becker, A., Finger, P., Meyer-Christoffer, A., Rudolf, B., & Ziese, M.
32 (2011a). GPCC Full Data Reanalysis Version 6.0 at 1.0°: monthly land-surface precipitation
33 from rain-gauges built on GTS-based and historic data.
34 doi:10.5676/DWD_GPCC/FD_M_V6_100

- 1
2 Schneider, U., Becker, A., Finger, P., Meyer-Christoffer, A., Rudolf, B., & Ziese, M.
3 (2011b). GPCC Monitoring Product Version 4.0 at 1.0°: near real-time monthly land-surface
4 precipitation from rain-gauges based on SYNOP and CLIMAT Data. doi: 10.5676/
5 DWD_GPCC/MP_M_V4_100
6
7 Schneider, U., Becker, A., Finger, P., Meyer-Christoffer, A., Ziese, M., & Rudolf, B. (2014).
8 GPCC's new land surface precipitation climatology based on quality-controlled in situ data
9 and its role in quantifying the global water cycle. *Theor. Appl. Climatol.* **115**: 15-40.
10
11 Seager, R., Harnik, N., Kushnir, Y., Robinson, W., & Miller, J. (2003). Mechanisms of
12 hemispherically symmetric climate variability. *J. Clim.* **16**: 2960-2978.
13
14 Sun, D., Xue, F., & Zhou, T. (2013). Impacts of two types of El Niño on atmospheric
15 circulation in the Southern Hemisphere. *Adv. Atmos. Sci.* **30**: 1732-1742.
16
17 Taschetto, A.S., Haarsma, R.J., Sen Gupta, A., Ummenhofer, C.C., Hill, K.J., & England
18 M.H. (2010). Australian monsoon variability driven by a Gill–Matsuno type response to
19 central western Pacific warming. *J. Clim.* **23**: 4717-4736.
20
21 Thom, H.C.S. 1958). A note on the Gamma Distribution. *Mon. Wea. Rev.* **86**(4): 117-122.
22
23 Thompson, D.W.J., & Wallace, J. (2000). Annular modes in the extratropical circulation. Part
24 I: Month-to-month variability. *J. Clim.* **13**: 1000-1016.
25
26 Todd, M.C., & Washington, R. (1999). Circulation anomalies with tropical-temperate troughs
27 in Southern Africa and the South West Indian Ocean. *Clim. Dyn.* **15**: 937-951.
28
29 Trenberth, K.E., Fasullo, J.T., & Mackaro, J. (2011). Atmospheric Moisture Transports from
30 Ocean to Land and Global Energy Flows in Reanalyses. *J. Clim.* **24**, 4907-4924
31
32 Tyson, P.D., Dyer, T.G.J., & Mametse, M.N. (1975). Secular changes in South African
33 rainfall: 1880 to 1972. *Q. J. R. Meteorol. Soc.* **101**: 817-833.
34

- 1 Vigaud, N., Richard, Y., Rouault, M., & Fauchereau, N. (2007). Water vapor transport from
2 the tropical Atlantic and summer rainfall in tropical southern Africa. *Clim. Dyn.* **28**: 113-123.
3
- 4 Washington, R., & Todd, M.C. (1999). Tropical-temperature links in Southern African and
5 Southwest Indian Ocean satellite-derived daily rainfall. *Int. J. Climatol.* **19**: 1602-1616.
6
- 7 Washington, R., & Preston, A. (2006). Extreme wet years over Southern Africa: role of
8 Indian Ocean Sea Surface Temperatures. *J. Geophys. Res.* **111**:
9 doi:10.1029/2005JD00672415.
10
- 11 Weng, H., Behera, S.K., & Yamagata, T. (2009). Anomalous winter climate conditions in the
12 Pacific rim during recent El Niño Modoki and El Niño events. *Clim. Dyn.* **32**: 663-674.
13
- 14 Wilson, A.B., Bromwich, D.H., Hines, K.M., & Wang, S-H. (2014). El Niño flavors and their
15 simulated impacts on atmospheric circulation in the high southern latitudes. *J. Clim.* **27**:
16 8934-8955.
17
- 18 Yamagata, T., Behera, S.K., Rao, S.A., Guan, Z., Ashok, K., & Saji, N.H. (2003). Comments
19 on “Dipoles, Temperature Gradient, and Tropical Climate Anomalies”, *Bull. Am. Meteorol.*
20 *Soc.* **84**: 1418–1422.
21
- 22 Yeh, S-W., Kug, J-S., Dewitte, B, Kwon, M-H., Kirtman, B.P., & Jin, F-F. (2009). El Niño in
23 a changing climate. *Nature*, **461**: 511-514.
24
- 25 Yu, J-Y., & Kim, S.T. (2013). Identifying the types of major El Niño events since 1870. *Int.*
26 *J. Climatol.* **33**: 2105-2112.
27
- 28 Zhang, Q., Körnich, H., & Holmgren, K. (2013). How well do reanalyses represent the
29 southern African precipitation? *Clim Dyn.* **40(3-4)**: 951-962.

List of Figures:

Figure 1: The figure depicts the location of key regional circulation features influencing the weather and climate of southern Africa that are described in the text. The location of the Angola Low during the summer period (using the threshold described in *Section 2*) is portrayed by the grey box labelled ‘AL’. The grey contours are the DJF mean sea level pressure, illustrating the position of the subtropical South Atlantic and South Indian Ocean High Pressure cells, while the vectors are the mean DJF 850 hPa moisture flux (in $\text{g.kg}^{-1} \text{ m.s}^{-1}$; scale in top right corner). The approximate location of the core of the Botswana High (labelled ‘BH’) at the 500 hPa level is depicted by the red ellipse. Also shown are the six mini-domains (red boxes) over South Africa from where the SAWS station data was available. These mini-domains are referred to as Limpopo (A), Gauteng (B), Free State (C), north coastal KwaZulu-Natal (KZN) (D); south coastal KZN (E) and the Eastern Cape (F).

Figure 2: Times series of the SST anomalies ($^{\circ}\text{C}$) in the Niño 3.4 region for the recent El Niño events (since 1982), starting from the January of the onset year (indicated by the “-1”). The three strongest El Niño events (1982/83, 1997/98 and 2015/16), which are used in this analysis, are highlighted in a grey dashed, black dashed and solid black line, respectively.

Figure 3: The top panels show the early summer (OND) 3-month SPI (shaded; drought intensity) in the GPCC rainfall for (a) 2015, (b) 1997 and (c) 1982. Similarly, the bottom panels are for the late summer (JFM) for (d) 2016, (e) 1998 and (f) 1983.

Figure 4: Intensity-Areal extent-Frequency (IAF) curves (see *Section 2* for details) estimated from the seasonal mean SPI over the southern Africa domain (10.5° - 35.5°S ; 10.5° - 39.5°E) for (a) SPI-3 over the OND season (b) SPI-6 over the ONDJFM season. On the y-axis is the SPI drought intensity and on the x-axis the spatial area extent as a percentage of the domain area. Solid lines show the IAF curves for the study El Niño event years and dotted lines show selected benchmark return periods of 100, 200 and 300 years in (a) and 50, 100, and 300 years in (b) shown as black, cyan and purple, respectively. The estimated return period of the IAF curve for the extreme El Niño 2015/16 is estimated from the closest match to the benchmark return period IAF curves (*Section 3*).

Figure 5: Standardized summer (ONDJFM) rainfall anomalies for the period 1950-2016 over six domains across the summer rainfall region of South Africa. The location of the domain is illustrated in Fig. 1 (panel numbering used here is consistent with the box labels). The values are derived from SAWS station data, with the number of stations available in each domain given in the top right hand corner of each panel. The ENSO events of 1982/83, 1997/98 and 2015/16 are highlighted with black shaded bars.

Figure 6: SST anomalies ($^{\circ}\text{C}$; shaded with contours at every 1°C interval) during the early austral summer months (OND) for (a) 2015, (b) 1997 and (c) 1982.

Figure 7: The early summer months (OND) 200 hPa geopotential height anomalies (m; contours) for (a) 2015/16, (b) 1997/98 and (c) 1982/83 El Niño events. Shading in panels a, b and c represents grid points that contain the same sign anomaly in all three panels. The OND composite of the Eastern Pacific El Niño events is given in panel d (m; shading with contours). Stippling in panel d indicates anomalies that are statistically significant at or above the 90% confidence level based on a t test.

Figure 8: Same as Fig. 7, but for the late summer months (JFM).

Figure 9: The (a) early summer (OND) and (b) late summer (JFM) 850 hPa mean weighted geopotential height anomaly (m) from within the Angola low domain (see Fig. 1). The triangle symbols on the top axis indicate El Niño or La Niña years, while the black bars highlight the 1982/83, 1997/98 and 2015/16 El Niño events.

Figure 10: 850hPa geopotential height anomalies (m; shaded) and moisture flux anomalies (vectors; $\text{g.kg}^{-1}.\text{m.s}^{-1}$) during El Niño events for (a) OND 2015, (b) OND 1997, (c) OND 1982, (d) JFM 2016, (e) JFM 1998 and (f) JFM 1983.

Figure 11: The early summer months (OND) 500 hPa geopotential height anomalies (m; contours) for (a) 2015/16, (b) 1997/98 and (c) 1982/83 El Niño events. Shading in panels a, b and c represents grid points that contain the same sign anomaly in all three panels. The letters 'BH' denote the position of the Botswana High in OND 2015 in panel a. The OND composite of the Eastern Pacific El Niño events is given in panel d (m; shading with contours). Stippling

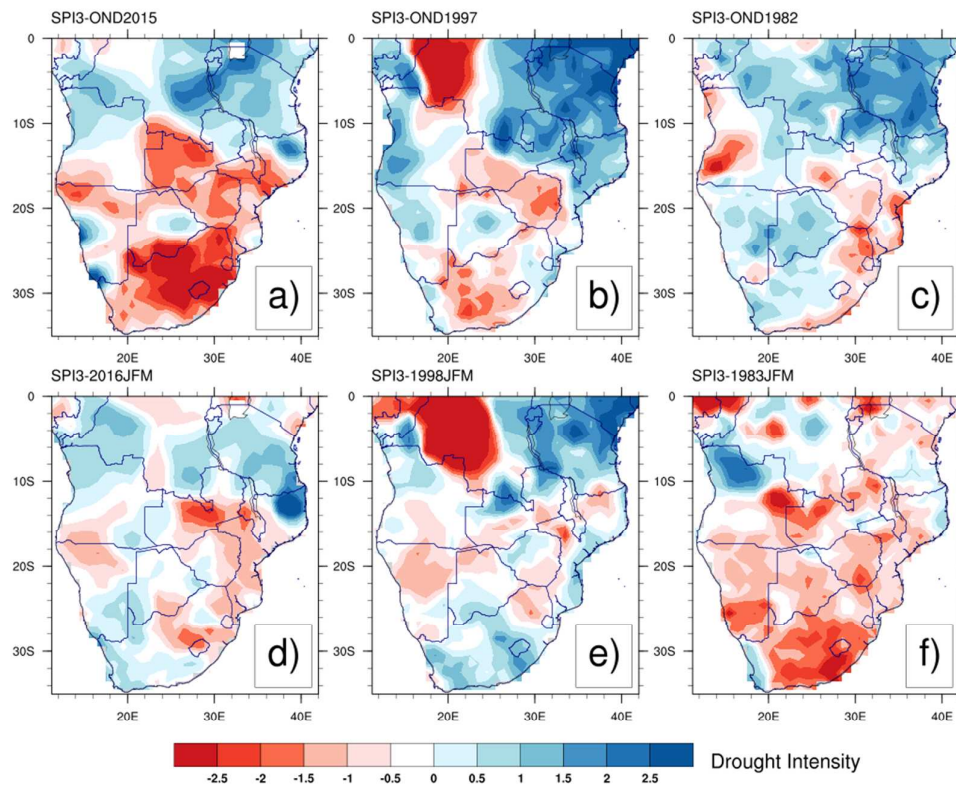
in panel d indicates anomalies that are statistically significant at or above the 90% confidence level based on a t test.

Figure 12: (a) Latitude-height cross section of Omega (Pa.s^{-1} ; shaded with contours) for the early summer (OND) mean and anomalies for the (b) 2015/16, (c) 1997/98 and (d) 1982/83 ENSO events. The panels on the right are for the (e) JFM mean and anomalies for the (f) 2015/16, (g) 1997/98 and (h) 1982/83 El Niño events. The values have been averaged along longitudes between 17.5° - 25.0°E . The thicker line along the x-axis in panels 'a' and 'e' is the latitudinal extent of the Angola low domain used.

Figure 13: Same as Fig. 11, but for the late summer months (JFM). The letters 'BH' denote the position of the Botswana High in JFM 1983 in panel c.

Title: The role of regional circulation features in regulating El Niño climate impacts over southern Africa: A comparison of the 2015/16 drought with previous events

Authors: R. C. Blamey*, S. R. Kolusu, P. Mahlalela, M.C. Todd and C. J. C. Reason



Extremely dry conditions (Standardized Precipitation Index shown above) were experienced across most of southern Africa during the austral summer (October-March) of 2015/16, associated with one of the strongest observed El Niño events in the Pacific. When comparing to past strong El Niño events, it is evident that key regional scale circulation patterns, influenced by planetary scale processes, play an important role in modulating the spatial and temporal evolution of the summer rainfall during these events.

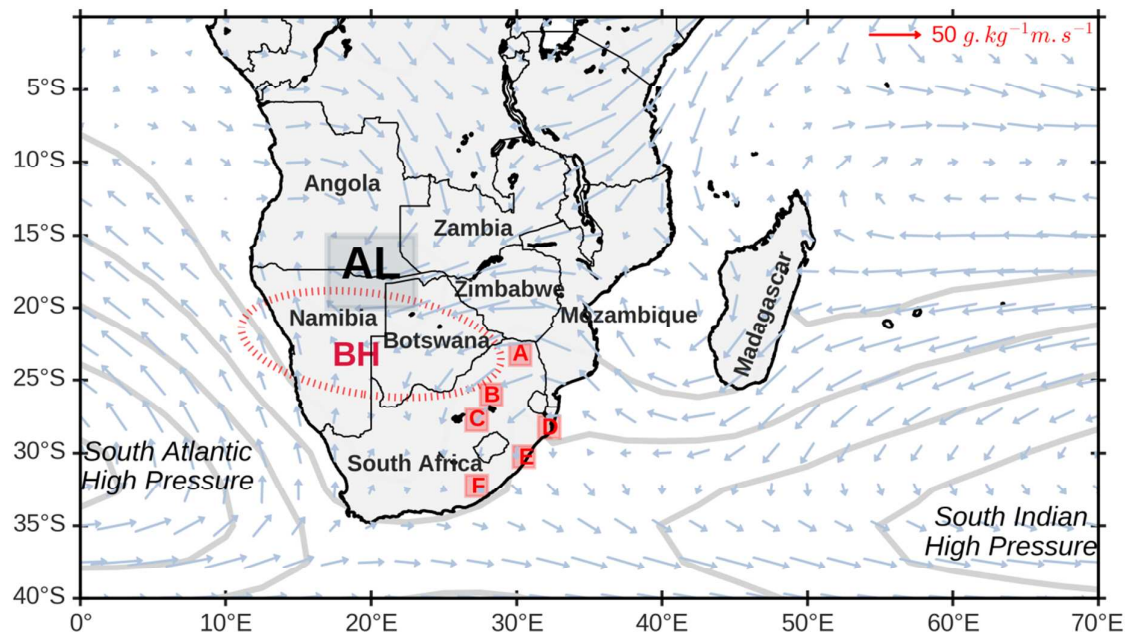


Figure 1: The figure depicts the location of the key regional circulation features influencing the weather and climate of southern Africa that are described in the text. The location of the Angola Low during the summer period (using the threshold described in *Section 2*) is portrayed by the grey box labelled ‘AL’. The grey contours are the DJF mean sea level pressure, illustrating the position of the subtropical South Atlantic and South Indian Ocean High Pressure cells, while the vectors are the mean DJF 850 hPa moisture flux ($\text{g.kg}^{-1} \text{m.s}^{-1}$; scale in top right corner). The approximate location of the core of the Botswana High (labelled ‘BH’) at the 500 hPa level is depicted by the red ellipse. Also shown are the six mini-domains (red boxes) over South Africa from where the SAWS station data was available. These mini-domains are referred to as Limpopo (A), Gauteng (B), Free State (C), north coastal KwaZulu-Natal (KZN) (D); south coastal KZN (E) and the Eastern Cape (F).

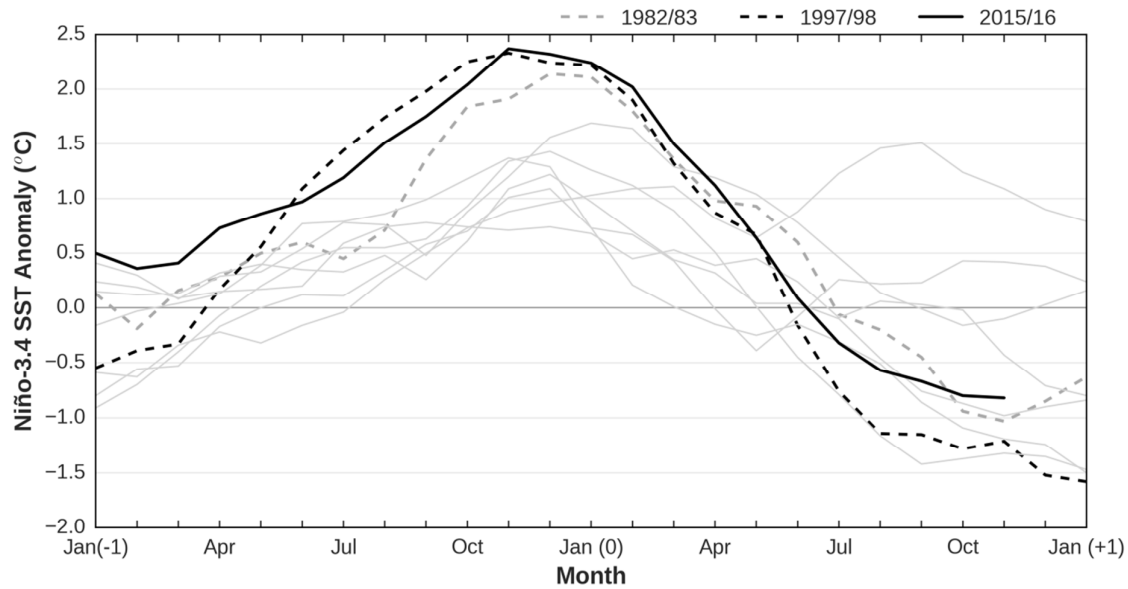


Figure 2: Times series of the SST anomalies ($^{\circ}\text{C}$) in the Niño 3.4 region for the recent El Niño events (since 1982), starting from the January of the onset year (indicated by the “-1”). The three strongest El Niño events (1982/83, 1997/98 and 2015/16), which are used in this analysis, are highlighted in a grey dashed, black dashed and solid black line, respectively.

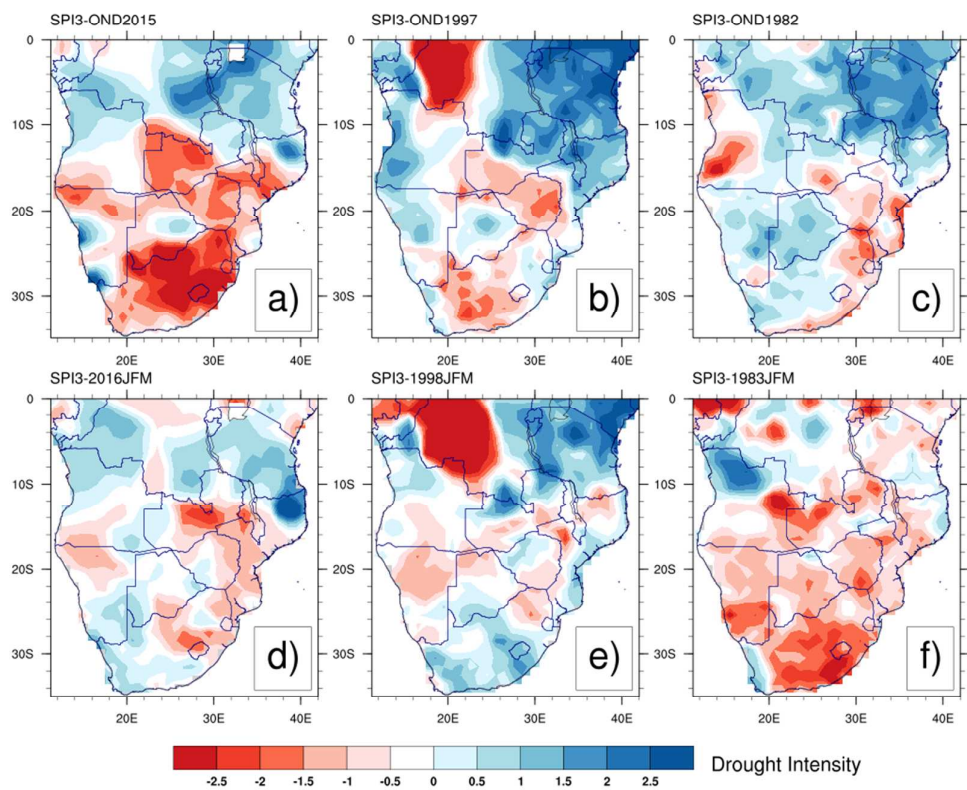


Figure 3: The top panels show the early summer (OND) 3-month SPI (shaded; drought intensity) in the GPCC rainfall for (a) 2015, (b) 1997 and (c) 1982. Similarly, the bottom panels are for the late summer (JFM) for (d) 2016, (e) 1998 and (f) 1983.

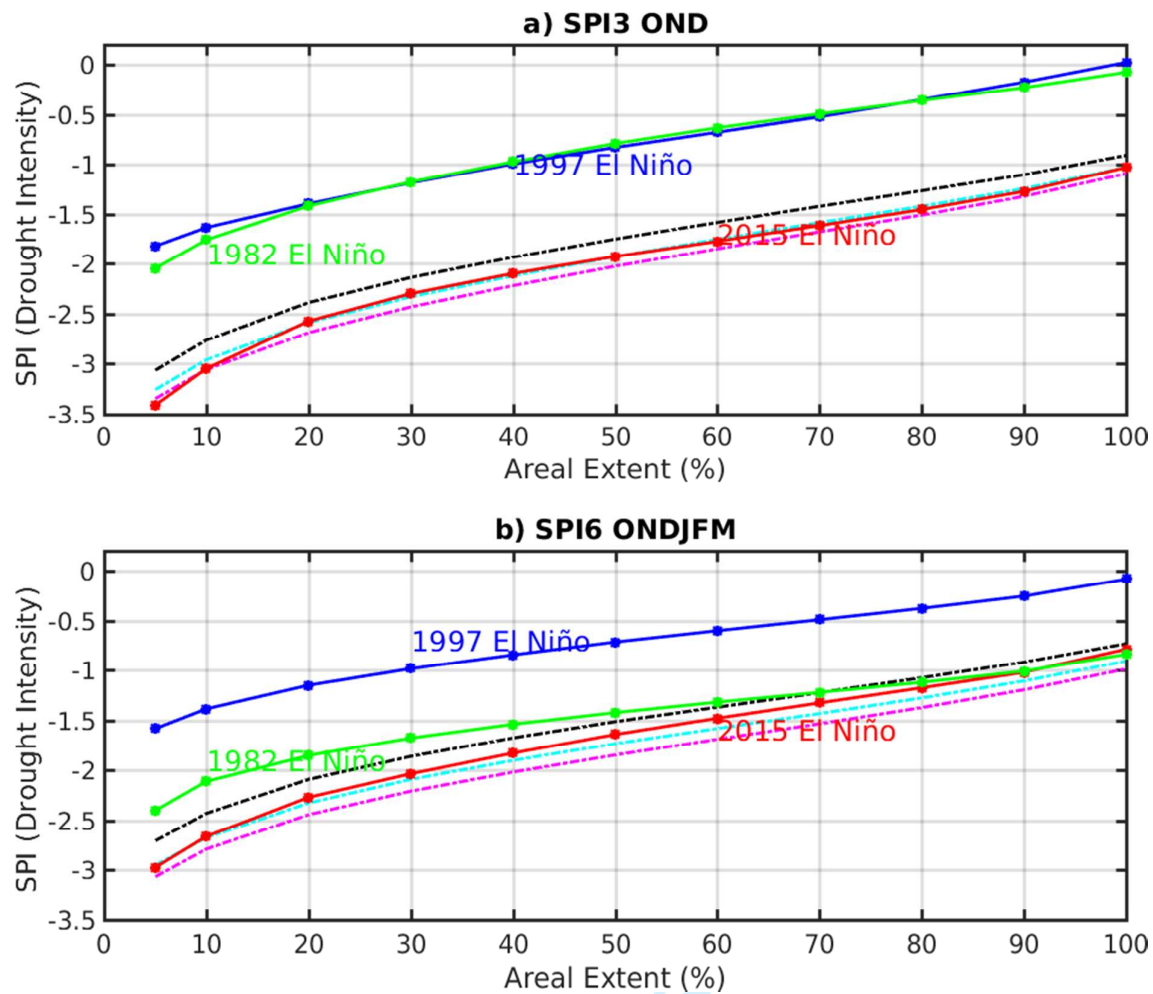


Figure 4: Intensity-Areal extent-Frequency (IAF) curves (see Section 2 for details) estimated from the seasonal mean SPI over the southern Africa domain (10.5° - 35.5° S; 10.5° - 39.5° E) for (a) SPI-3 over the OND season (b) SPI-6 over the ONDJFM season. On the y-axis is the SPI drought intensity and on the x-axis the spatial area extent as a percentage of the domain area. Solid lines show the IAF curves for the study El Niño event years and dotted lines show selected benchmark return periods of 100, 200 and 300 years in (a) and 50, 100, and 300 years in (b) shown as black, cyan and purple, respectively. The estimated return period of the IAF curve for the extreme El Niño 2015/16 is estimated from the closest match to the benchmark return period IAF curves (Section 3).

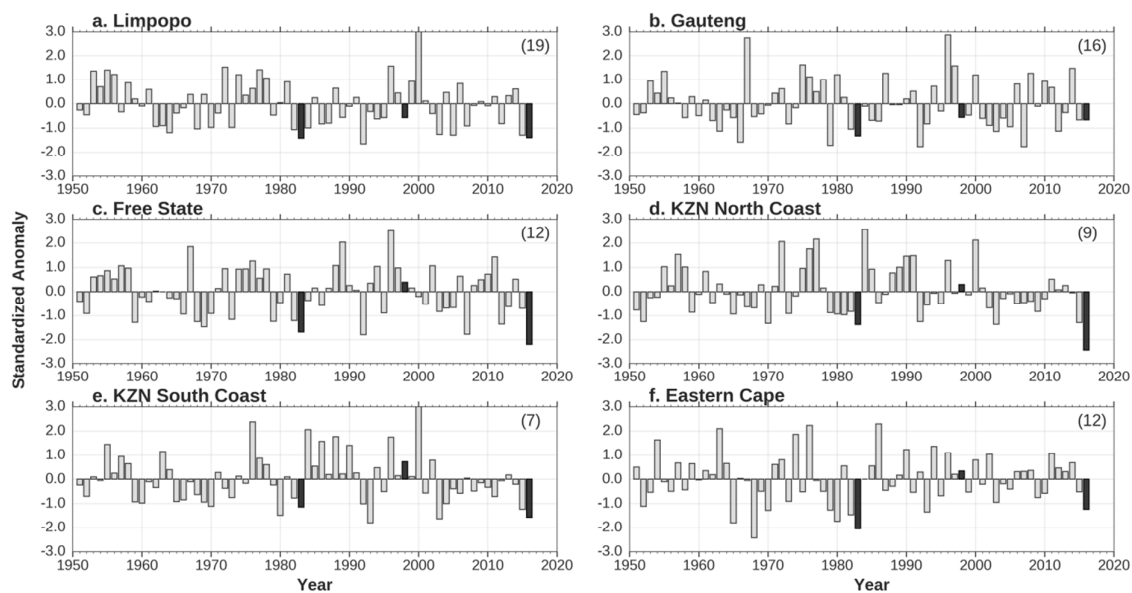


Figure 5: Standardized summer (ONDJFM) rainfall anomalies for the period 1950-2016 over six domains across the summer rainfall region of South Africa. The location of the domain is illustrated in Fig. 1 (panel numbering used here is consistent with the box labels). The values are derived from SAWS station data, with the number of stations available in each domain given in the top right hand corner of each panel. The ENSO events of 1982/83, 1997/98 and 2015/16 are highlighted with black shaded bars.

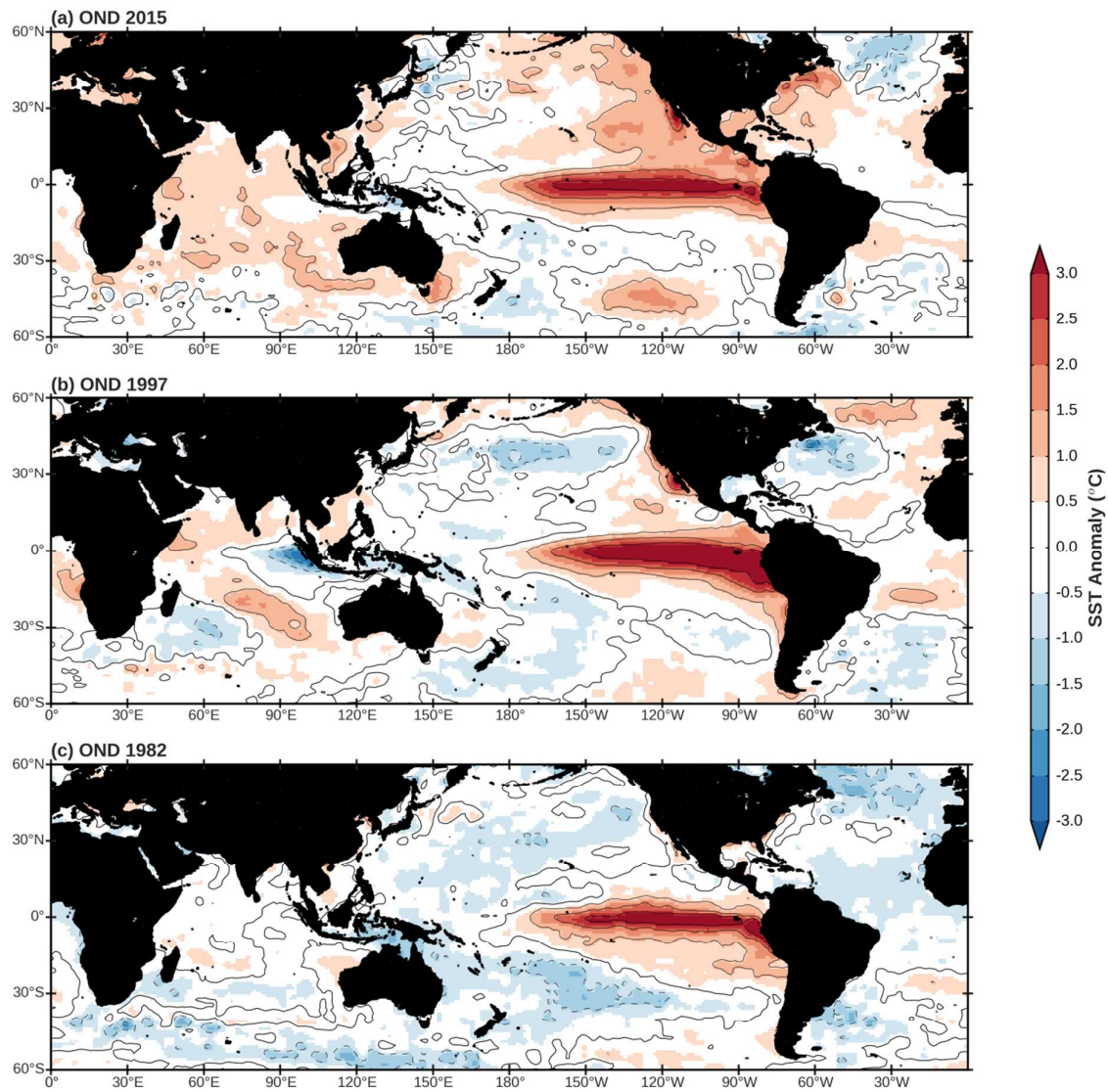


Figure 6: SST anomalies (°C; shaded with contours at every 1°C interval) during the early austral summer months (OND) for (a) 2015, (b) 1997 and (c) 1982.

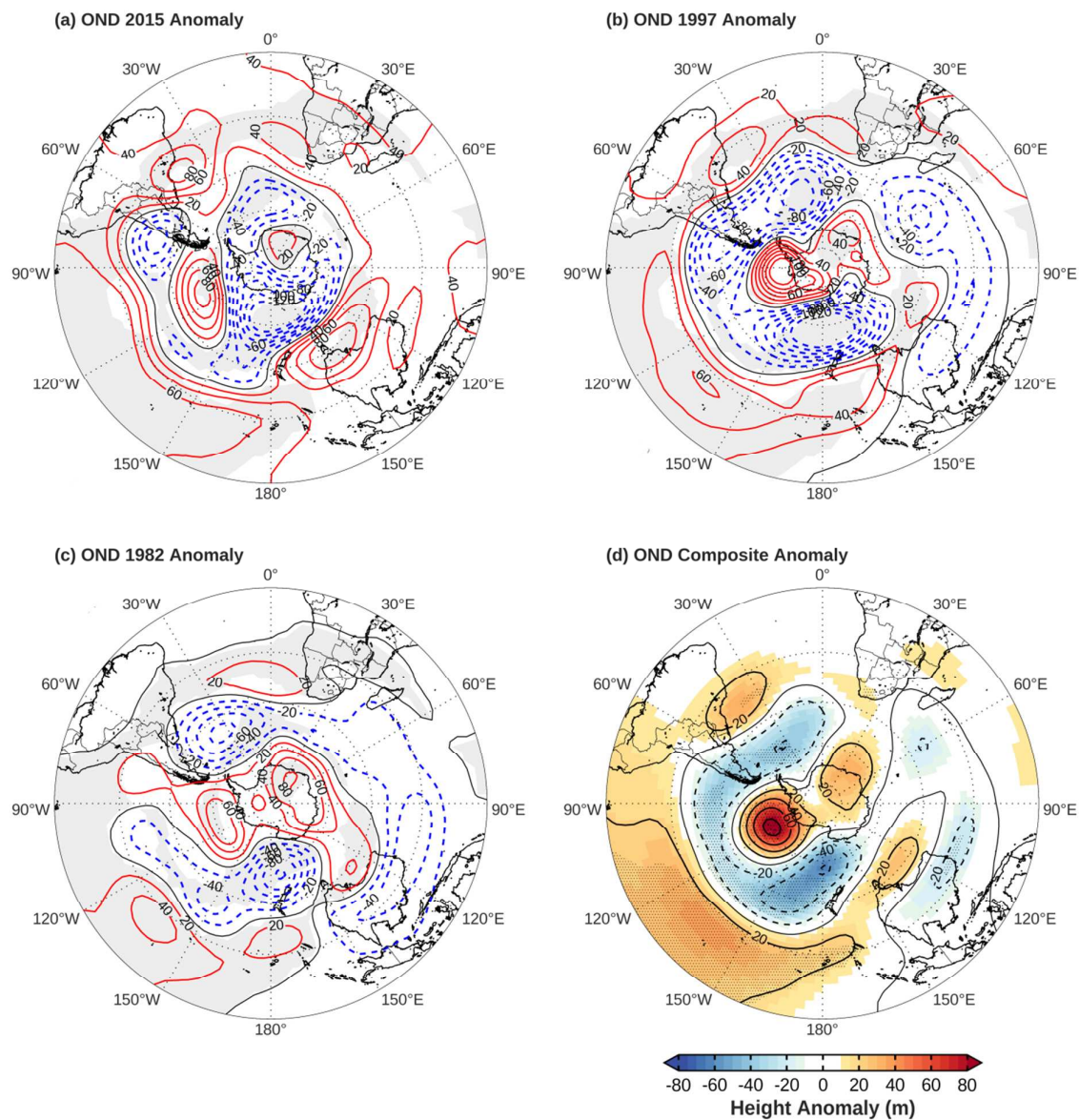


Figure 7: The early summer months (OND) 200 hPa geopotential height anomalies (m; contours) for (a) 2015/16, (b) 1997/98 and (c) 1982/83 El Niño events. Shading in panels a, b and c represents grid points that contain the same sign anomaly in all three panels. The OND composite of the Eastern Pacific El Niño events is given in panel d (m; shading with contours). Stippling in panel d indicates anomalies that are statistically significant at or above the 90% confidence level based on a *t* test.

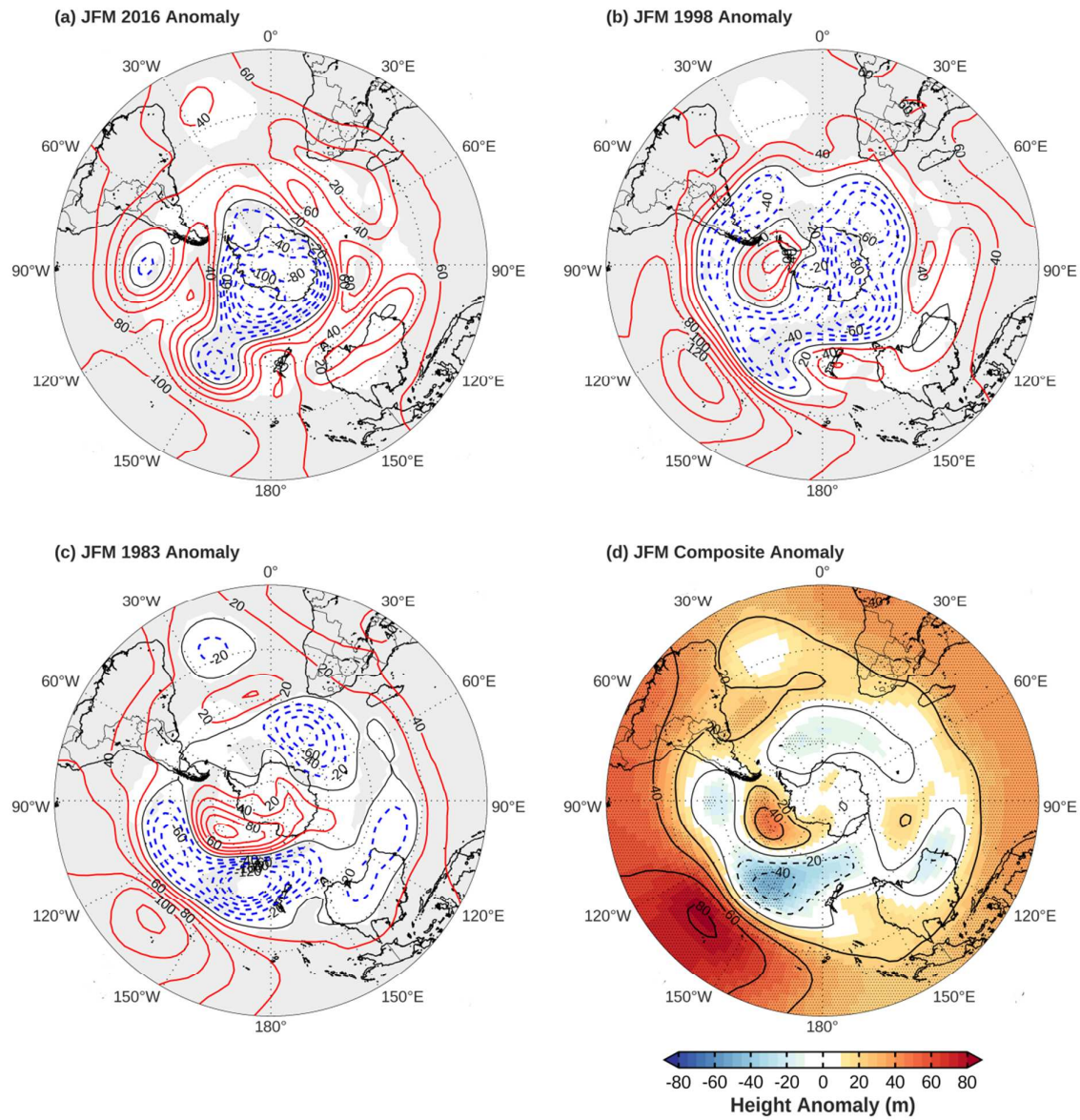


Figure 8: Same as Fig. 7, but for the late summer months (JFM).

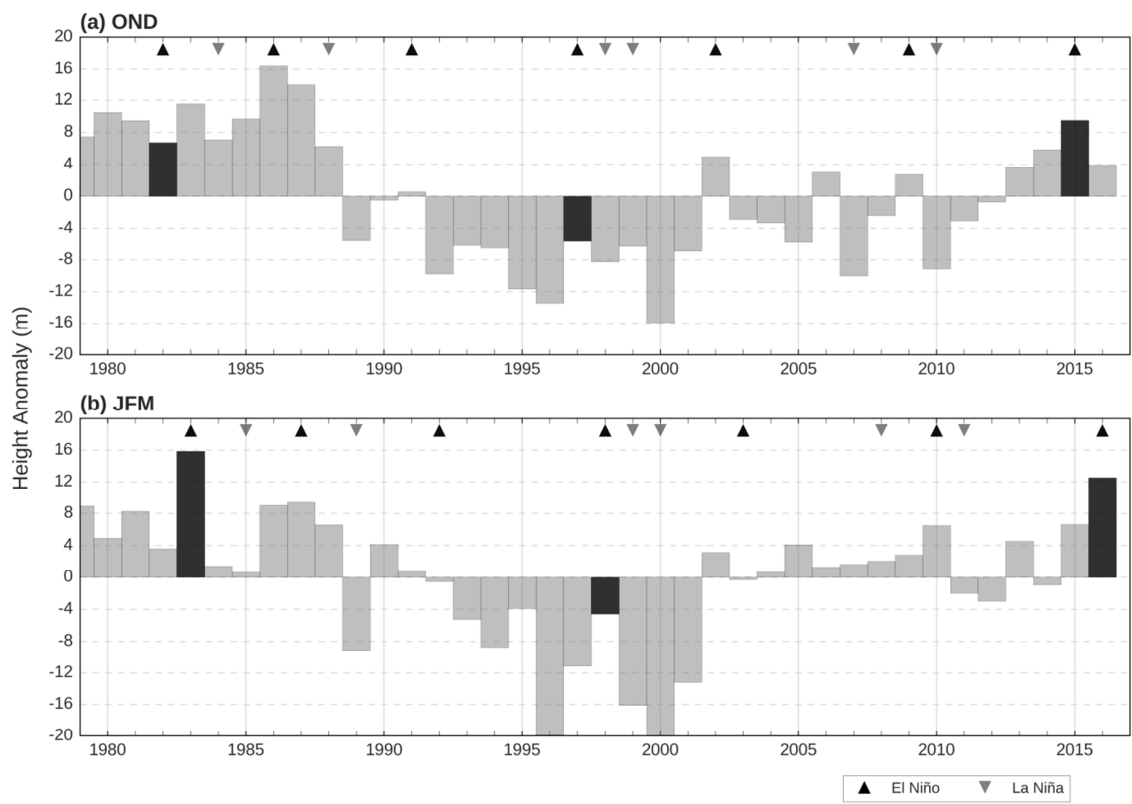


Figure 9: The (a) early summer (OND) and (b) late summer (JFM) 850 hPa mean weighted geopotential height anomaly (m) from within the Angola low domain (see Fig. 1). The triangle symbols on the top axis indicate El Niño or La Niña years, while the black bars highlight the 1982/83, 1997/98 and 2015/16 El Niño events

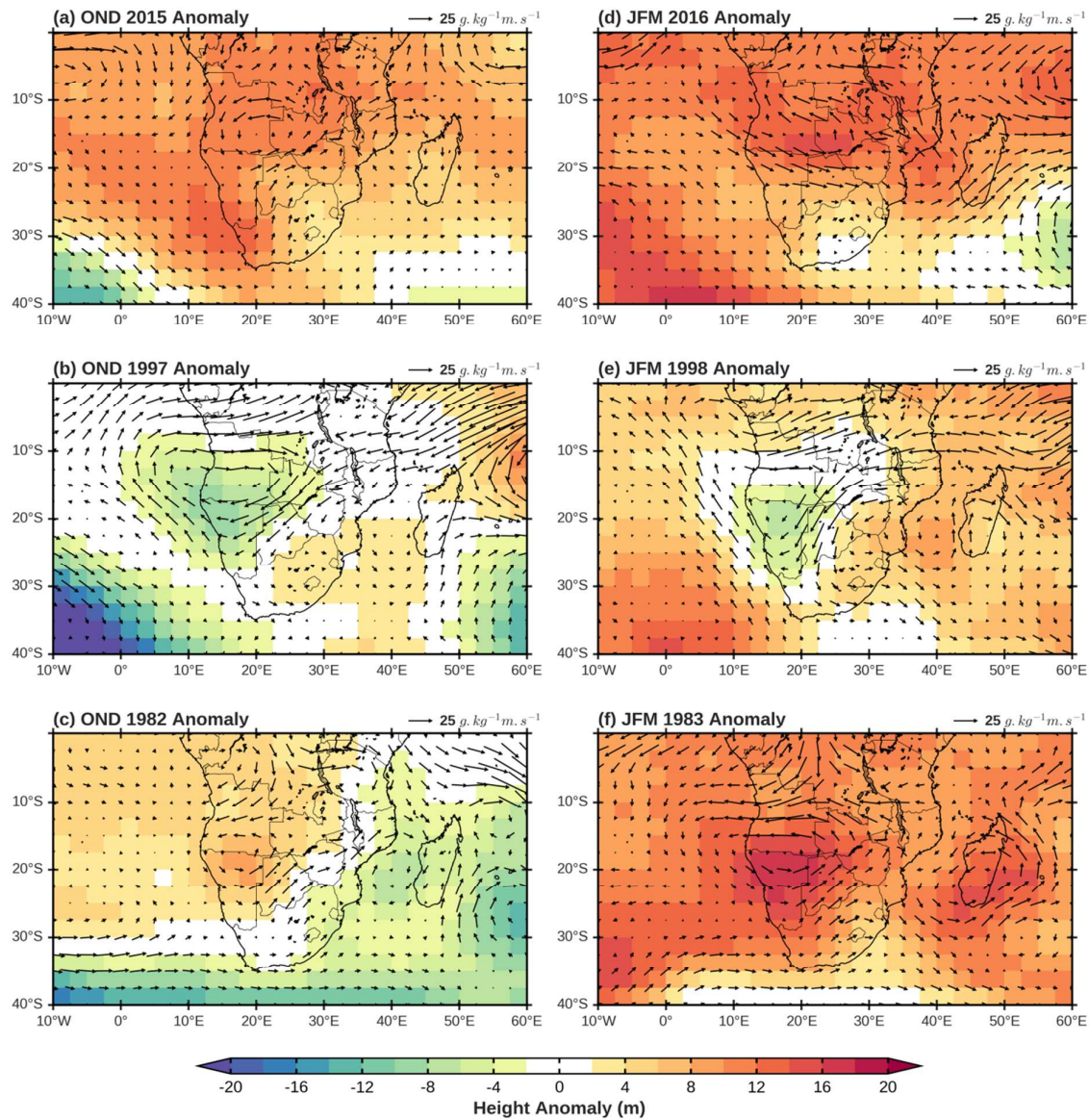


Figure 10: 850hPa geopotential height anomalies (m; shaded) and moisture flux anomalies (vectors; $g \cdot kg^{-1} \cdot m \cdot s^{-1}$) during El Niño events for (a) OND 2015, (b) OND 1997, (c) OND 1982, (d) JFM 2016, (e) JFM 1998 and (f) JFM 1983.

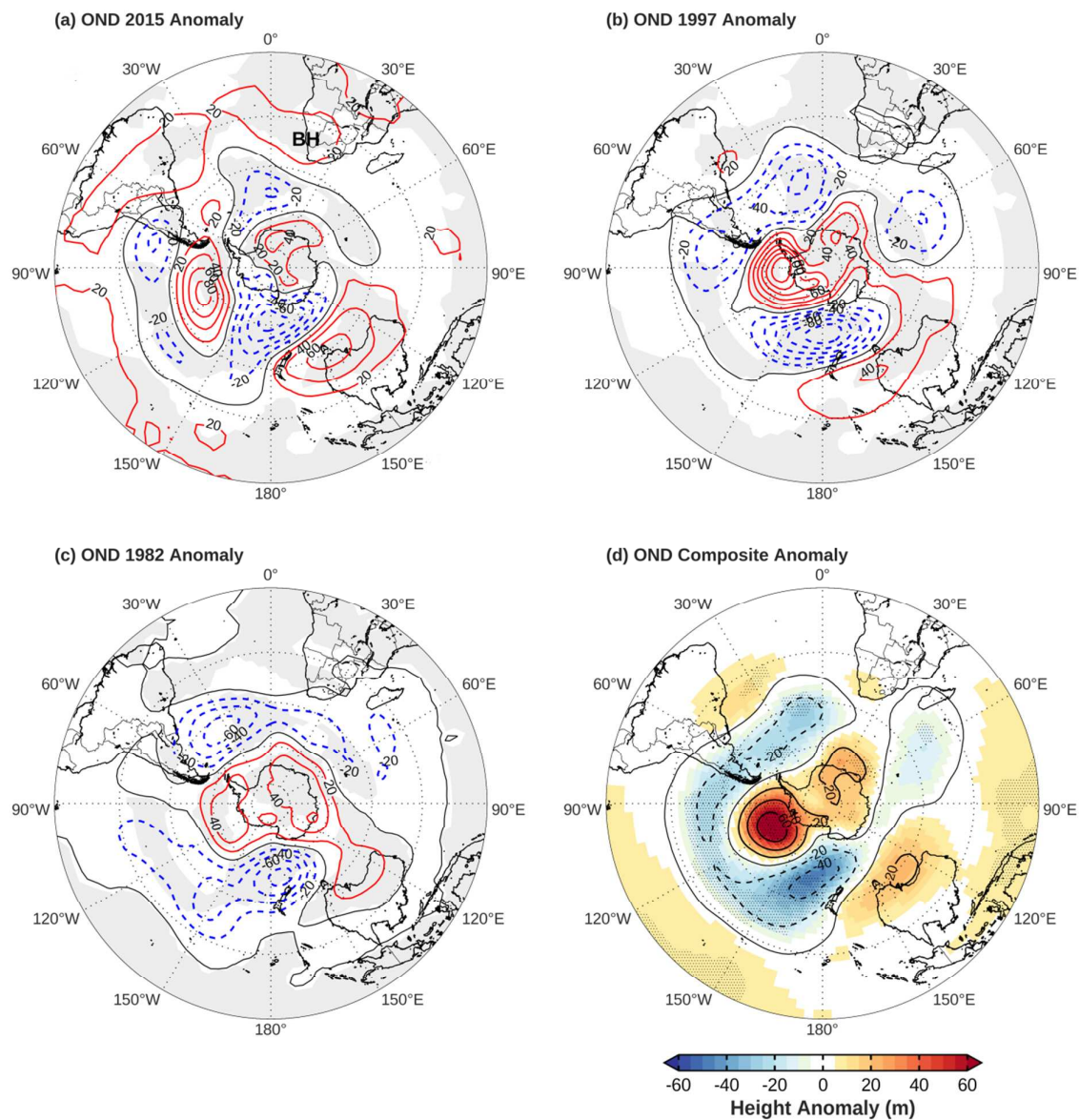


Figure 11: The early summer months (OND) 500 hPa geopotential height anomalies (m; contours) for (a) 2015/16, (b) 1997/98 and (c) 1982/83 El Niño events. Shading in panels a, b and c represents grid points that contain the same sign anomaly in all three panels. The letters ‘BH’ denote the position of the Botswana High in OND 2015 in panel a. The OND composite of the Eastern Pacific El Niño events is given in panel d (m; shading with contours). Stippling in panel d indicates anomalies that are statistically significant at or above the 90% confidence level based on a *t* test.

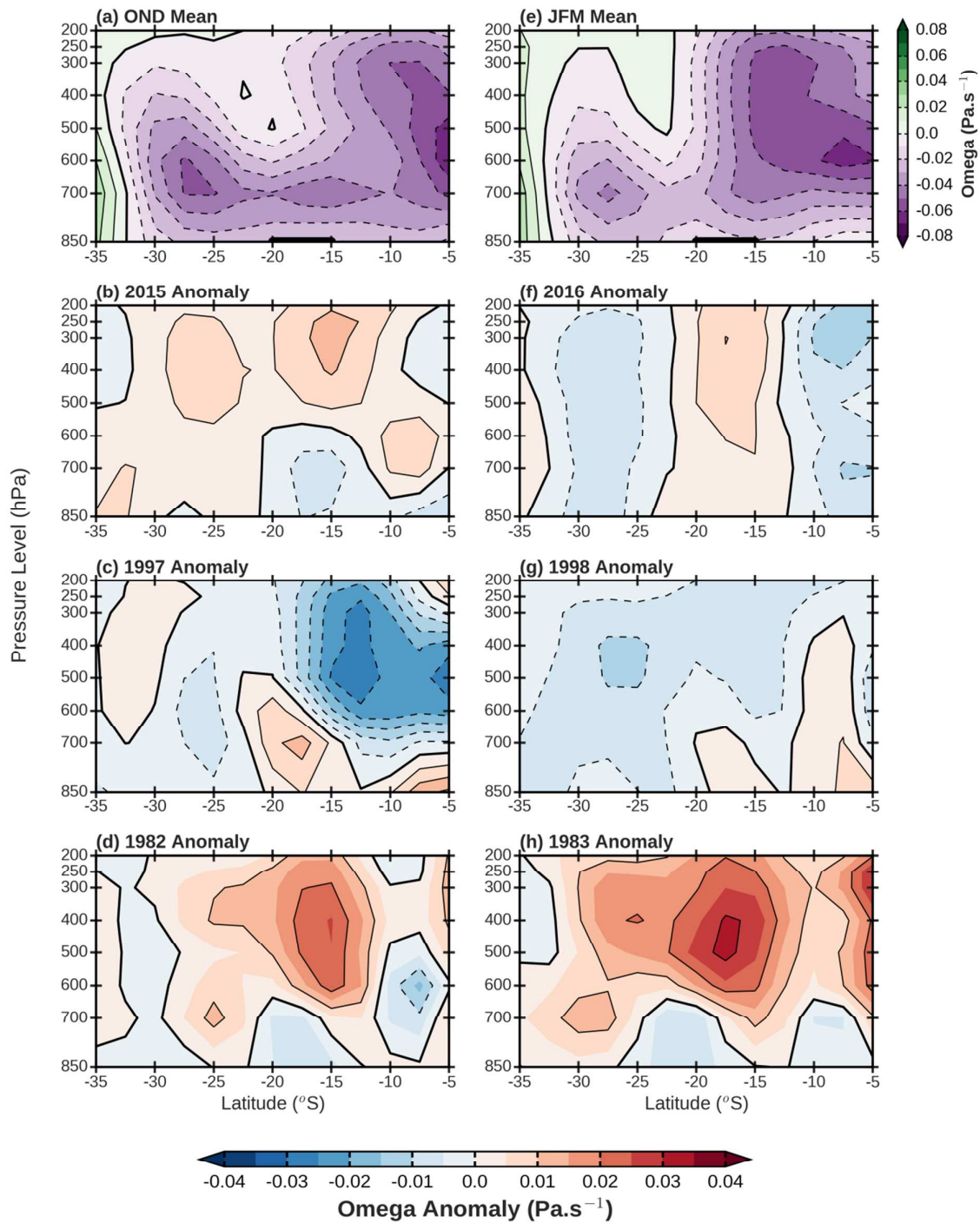


Figure 12: (a) Latitude-height cross section of Omega (Pa.s^{-1} ; shaded with contours) for the early summer (OND) mean and anomalies for the (b) 2015/16, (c) 1997/98 and (d) 1982/83 ENSO events. The panels on the right are for the (e) JFM mean and anomalies for the (f) 2015/16, (g) 1997/98 and (h) 1982/83 El Niño events. The values have been averaged along

longitudes between 17.5°-25.0°E. The thicker line along the x-axis in panels 'a' and 'e' is the latitudinal extent of the Angola low domain used.

Peer Review Only

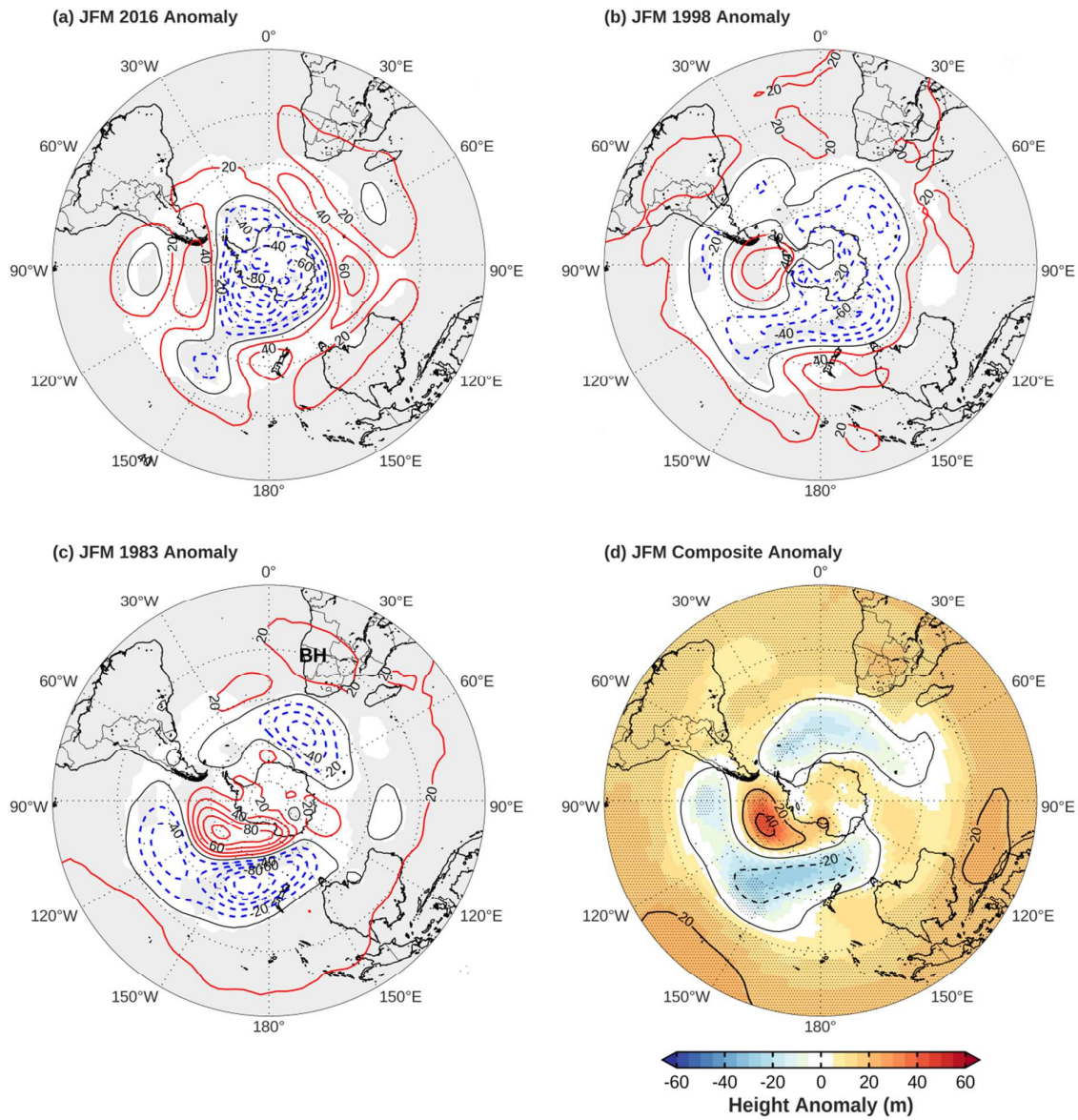


Figure 13: Same as Fig. 11, but for the late summer months (JFM). The letters 'BH' denote the position of the Botswana High in JFM 1983 in panel c.